What Fractionates Oxygen Isotopes During Respiration? Insights from Multiple Isotopologues and Theory

Jeanine L. Ash[1]*

Huanting Hu[1,2]

Laurence Yeung[1]

[1] Department of Earth, Environmental and Planetary Sciences, Rice University, Houston, TX 77005 USA

[2] Now at Institute of Oceanography, Shanghai Jiao Tong University, Shanghai 200242, China

[*]corresponding author

ABSTRACT: The precise mass dependence of respiratory O_2 consumption underpins the "oxygen triple-isotope" approach to quantifying gross primary productivity in modern and ancient environments. Yet, the physical-chemical origins of the key $^{18}O/^{16}O$ and $^{17}O/^{16}O$ covariations observed during respiration have not been tied to theory; thus the approach remains empirical. First-principles calculations on enzyme active-site models suggest that changes in the O-O bond strength upon electron transfer strongly influence respiratory isotopic fractionation.

1

However, molecular diffusion may also be important. Here, we use measurements of the relative abundances of rare isotopologues $^{17}O^{18}O$ and $^{18}O^{18}O$ as additional tracers of mass dependence during dark respiration experiments of lacustrine water. We then compare the experimental results to first-principles calculations of O_2 interacting with heme-oxidase analogues. We find a significantly steeper mass dependence, supported by theory, than has been previously observed. Enrichments of $^{17}O^{18}O$ and $^{18}O^{18}O$ in the O_2 residue suggest that θ values are strongly influenced by chemical processes, rather than being dominated by physical processes (i.e. by bond alteration rather than diffusion). In contrast, earlier data are inconsistent with theory, implying that analytical artifacts may have biased those results. Implications for quantifying primary productivity are discussed.

Introduction

The isotopic composition of molecular oxygen in Earth's atmosphere is determined by chemical reactions associated with biological and photochemical O_2 cycling.[1] Molecular oxygen is produced as a byproduct of photosynthesis, and its isotopic composition reflects that of its source waters [2-4]. Respiration preferentially consumes the lighter isotopes of oxygen, leaving behind a residue enriched in ^{18}O relative to meteoric waters.[2, 3, 5-12]. This difference between the oxygen-isotope composition of water and atmospheric O_2 due to biological fractionation is known as the Dole Effect.[6]

Prior to the late 1990's, work on attributing oxygen's isotope composition to biological processing centered on the most abundant rare isotope, ^{18}O. However, the inability to fully account for the magnitude of the Dole Effect and the discovery of mass-independent isotope effects arising from stratospheric photochemistry inspired the development of a "triple-isotope" parameter to further constrain oxygen biogeochemistry[13-15] This parameter, $\Delta'^{17}O$, exploits the

2

covariations in $\delta^{18}O$ and $\delta^{17}O$ values (i.e., $^{18}O/^{16}O$ and $^{17}O/^{16}O$ ratios; see below) that arise as different biogeochemical processes fractionate a pool of oxygen. While $\delta^{17}O$ values typically change about half as much as $\delta^{18}O$ values, mixing of O_2 from different sources can yield variability in $\Delta'^{17}O$ values that can be inverted to determine the isotopic mass balance.

Using these basic ideas, Luz and coworkers normalized $\Delta'^{17}O$ values of dissolved O_2 against experimental $\delta^{17}O/\delta^{18}O$ trends for respiration to partition photosynthetic and atmospheric O_2 in the oceanic mixed layer.[16] This approach to solving the mixed-layer O_2 mass balance yielded a now-widely-used tracer for marine gross oxygen productivity (GOP).[17-22] It was also applied to constrain past global biosphere productivity using O_2 trapped in ice cores.[23-25]

Recent work, however, suggests that the empirical $\delta^{17}O/\delta^{18}O$ trends for respiratory oxygen consumption are incompletely known. The potential for environmentally-forced variability in these trends and analytical artifacts, in particular, result in poorly characterized systematic uncertainties that could have significant effects on GOP estimates: errors of 10-15% in GOP are expected for every 0.001 error in the respiratory $\delta^{17}O/\delta^{18}O$ trend.[22, 26, 27]

The high sensitivity of GOP estimates to the assumed respiratory $\delta^{17}O/\delta^{18}O$ trend motivates this study. Can new measurements and first-principles theory be used to ground-truth observed trends?

Recently, it has become possible to quantify the abundances of doubly substituted O_2 isotopologues, i.e., $^{17}O^{18}O$ and $^{18}O^{18}O$.[28] The ability to measure these "clumped" isotopologues of O_2 allows one to observe multiple isotopologue covariations for the same process, providing additional constraints on the factors controlling isotopic fractionation in biogeochemical systems. Recent experiments, for example, showed that air-water gas exchange expresses isotopologue covariations similar to that for interdiffusion of O_2 through water molecules.[29]

In this paper, we report new triple- and clumped-isotope covariations in dark respiration experiments and compare these observations to those calculated for specific physical and chemical phenomena. We find that previously reported respiratory $\delta^{17}O/\delta^{18}O$ trends may be significantly in error: they cannot be reconciled with theory and our clumped-isotope constraints. However, $\delta^{17}O/\delta^{18}O$ trends that are steeper than previously thought can be reconciled with our results. Keeping all else equal, these steeper $\delta^{17}O/\delta^{18}O$ trends imply that marine GOP has been overestimated by up to ~40%. Revising the triple-isotope contrast between atmospheric O_2 and ocean water (the main source of photosynthetic O_2 for marine GOP) to the most recent value [30, 31] would reduce these overestimates. Our findings highlight a need to evaluate these and other similar empirical parameters in the context of first-principles theory.

Isotopic notation

We will provide a brief review of stable isotope notation before detailing the relationships between two isotopes or isotopologues during fractionation. Because the fractionation of oxygen isotopes during respiration is the primary focus, we will use notation specific to this topic as examples of these broader concepts. More general examples of these equations can be found elsewhere.[32, 33] First, R describes the ratio of minor isotopes (i.e. ^{18}O or ^{17}O) to a more abundant isotope (^{16}O), and δ-notation quantifies the difference of these ratios between an analyte sample and standard, reported in per mil (‰).

(1)
$$\delta^{18}O = \left(\frac{^{18}R_{\text{sample}}}{^{18}R_{\text{standard}}} - 1 \right)$$

Herein, we use atmospheric O_2 as the primary standard. During a process such as respiration, the fractionation of isotopes between two phases, materials or reservoirs (i.e., respired oxygen and the remaining residue of oxygen) is described using α notation.

$$(2) \qquad {}^{18}\alpha_{\text{Respired } O_2 \text{-Residual } O_2} = \frac{{}^{18}R_{\text{Respired } O_2}}{{}^{18}R_{\text{Residual } O_2}}$$

We note here that in some biogeochemical studies, ε notation has also been used to describe isotope discrimination during fractionation, i.e.,

$$(3) \qquad \varepsilon_{\text{Respired } O_2 \text{- Residual } O_2} = {}^{18}\alpha_{\text{Respired } O_2 \text{- Residual } O_2} - 1 .^{10}$$

During a mass-dependent process, isotopic species fractionate in a co-varying manner related by the quantity θ.

$$(4) \qquad {}^{17}\alpha = \left({}^{18}\alpha \right)^{\theta}$$

It is often beneficial to linearize these equations to simplify mathematical operations, so the following expressions can be used in lieu of Equations 1-3:

$$(5) \qquad \delta'^{18}O = \ln\left(\frac{{}^{18}R_{\text{sample}}}{{}^{18}R_{\text{standard}}} \right)$$

$$(6) \qquad \ln\left({}^{18}\alpha_{\text{Respired } O_2 \text{-Residual } O_2} \right) = \ln\left(\frac{{}^{18}R_{\text{Respired } O_2}}{{}^{18}R_{\text{Residual } O_2}} \right)$$

5

(7)
$$\ln(^{17}\alpha) = \theta \ln(^{18}\alpha)$$

The linearized notation is distinguished by the inclusion of a prime (′) symbol. Expressions for θ can thus be determined as

(8)
$$\theta_{17/18} = \frac{\ln(^{17}\alpha)}{\ln(^{18}\alpha)}$$

Finally, one may be interested in relating a substance's isotopic composition to an expected composition predicted by a theoretical or empirical mass-dependent relationship. Here, we use "λ" in place of "θ" to highlight that this value is often an empirically derived relationship (i.e. the terrestrial fractionation line or closed-system respiration).

(9)
$$\Delta'^{17}O = \delta'^{17}O - \lambda_{17/18} \times \delta'^{18}O$$

The measure of the substance's departure from expectation, $\Delta'^{17}O$ (reported in parts per million, ppm), has been applied to many systems both terrestrial and planetary, and we note that other communities may refer to this parameter as "^{17}O-excess" or the entire system as "triple oxygen isotopes."[15, 34-38] The value $\lambda_{17/18} = 0.518$ is typically used for marine GOP studies.[21, 39]

θ values in singly substituted isotopologues can be variable

Mass-dependent processes typically fractionate $\delta'^{17}O$ values approximately half as much as $\delta'^{18}O$ values; therefore, θ is ~0.5. Subtle deviations from this nominal value may be used as a process diagnostic. For example, the rates of kinetic processes may scale with atomic or molecular velocity (e.g., particle mass for diffusion-limited processes). Hence, the θ values of certain kinetic processes can be approximated using the atomic or molecular mass of oxygen in Eq. 10:

6

$$(10) \qquad \theta_{17/18,\,kinetic} = \frac{\ln\left(\dfrac{m_{16}}{m_{17}}\right)}{\ln\left(\dfrac{m_{16}}{m_{18}}\right)}$$

where m is an atomic or molecular mass and subscripts refer to the three stable oxygen isotopes (^{16}O, ^{17}O, ^{18}O) or stable O_2 isotopologues ($^{16}O^{16}O$, $^{16}O^{17}O$, $^{16}O^{18}O$, $^{17}O^{17}O$, $^{17}O^{18}O$ and $^{18}O^{18}O$). Solving Eq. 10 using these respective mass values yields $\theta_{17/18,\,kinetic} = 0.516$ and $\theta_{33/34,\,kinetic} = 0.509$ for atomic and molecular oxygen, respectively (subscripts indicate the cardinal mass of the species in the numerator and denominator of Eq. 9, respectively).

In contrast, equilibrium processes depend on the thermodynamics of bonds in the coexisting species.[40, 41] The θ values associated with equilibrium processes are typically temperature-dependent, but at the high-temperature limit they approach the following value:

$$(11) \qquad \theta_{17/18,\,equilbrium} = \frac{\left(\dfrac{1}{m_{16}} - \dfrac{1}{m_{17}}\right)}{\left(\dfrac{1}{m_{16}} - \dfrac{1}{m_{18}}\right)}\ .$$

The expression above was originally derived assuming that vibrations are harmonic, but it has nevertheless proven to be a good guidepost in a variety of systems.[32, 33] Solving Equation 11 using the exact masses for atomic oxygen yields $\theta = 0.5305$.

Specific processes differ subtly in their fractionation tendencies, however, complicating the simple view presented above.[32, 33, 42, 43] For example, the θ value most frequently associated with dark respiration lies between 0.514 and 0.516.[12, 44] This constant was empirically determined for a range of organisms and found to be nearly invariant despite much larger variability in $^{18}\varepsilon$ values. Why this θ value appeared universal for dark respiration remains unclear: other

processes, such as the diffusion of O_2 to the site of respiration, the reversible binding of O_2 to an enzyme, and the irreversible reduction of O_2 to water may be variably expressed in different organisms and different environments, potentially leading to deviations from the canonical range.

Indeed, Stolper et al. (2018) found that respiratory $\theta_{17/18}$ values increased with temperature in axenic cultures of *Escherichia coli* grown between 15°C and 37°C. These $\theta_{17/18}$ values ranged from 0.508 to 0.513, which are all significantly lower than the canonical range. No effects were observed from altering the electron donor. They hypothesized that the trend arises from a shifting balance between O_2-enzyme binding and O_2 reduction and constructed a two-step model for $\theta_{17/18}$ values and bulk-isotope fractionation that explained their data. While the specific boundary conditions in that model remain to be tested, the newfound variability in respiratory $\theta_{17/18}$ values raises questions about the accuracy of $\theta_{17/18}$ values used in GOP estimates.

Accurate $\theta_{17/18}$ values are crucial for determinations of GOP

The precise value of $\theta_{17/18}$ (and $\lambda_{17/18}$) for respiration in natural systems is one of three elements that must be determined independently for triple-isotope-based estimates of GOP. The others are the isotopic composition of atmospheric O_2 dissolved in water at equilibrium and the isotopic fractionation for photosynthetic O_2 production from water. Together, these elements allow one to construct a mass balance of O_2 within the oceanic mixed layer. A brief description of the method follows.

Atmospheric O_2 has a unique $\Delta'^{17}O$ value inherited from mass-independent isotope exchange during photochemical reactions between CO_2, O_3 and O_2 in the stratosphere.[15, 45, 46] This value is distinct from that produced by photosynthesis, the other main source of O_2 in the surface ocean.[3, 4] At its simplest, dissolved O_2 is the combination of these two sources, and $\Delta'^{17}O$ can be used as a

tracer of the mass balance between them. Respiration and gas exchange with the atmosphere are additional processes that influence $\Delta'^{17}O$ and must be accounted for. Using a $\lambda_{17/18}$ value of 0.518 preserves the $\Delta'^{17}O$ of O_2 during respiration in principle, while gas exchange tends to drive the dissolved O_2 composition toward solubility equilibrium (Figure 1a).[21]

The method has been instrumental in assessing open-ocean GOP over the past two decades, offering a valuable spatiotemporal bridge between traditional short-term incubation methods and regional-to-global satellite estimates derived from ocean color.[16, 18, 47-49] Each method has its unique uncertainties.[19, 50-52] Yet as the triple-isotope field has matured, it has become clear that many factors can exert a significant influence on $\Delta'^{17}O$-based estimates of productivity, e.g., uncertainties in gas exchange rates and isotopic perturbations associated with non-steady-state conditions variable expression of respiration mechanisms and their fractionation factors; the source-water isotopic composition; and mathematical approximations used in calculations. [3, 12, 22, 26, 29, 53-60]

To the best of our knowledge, however, the origin of the $\lambda_{17/18}$ value of 0.518 has not been studied. It is consistent with the accepted range of $\theta_{17/18}$ values measured for dark respiration (0.514 – 0.516) and lies close to that from the simplified calculation for kinetic fractionation (see Eq. 10).[12, 23, 44] Yet a clear mechanism that explains this trend, rooted in physical and/or biochemical processes, has been lacking. The potential interplay of diffusion, O_2-enzyme interactions, and O_2 reduction kinetics in the expression of isotopic fractionation suggests that multiple factors could be important for determining the respiratory $\theta_{17/18}$ value. Without a mechanistic understanding, however, the systematic uncertainty in GOP estimates will remain poorly known.
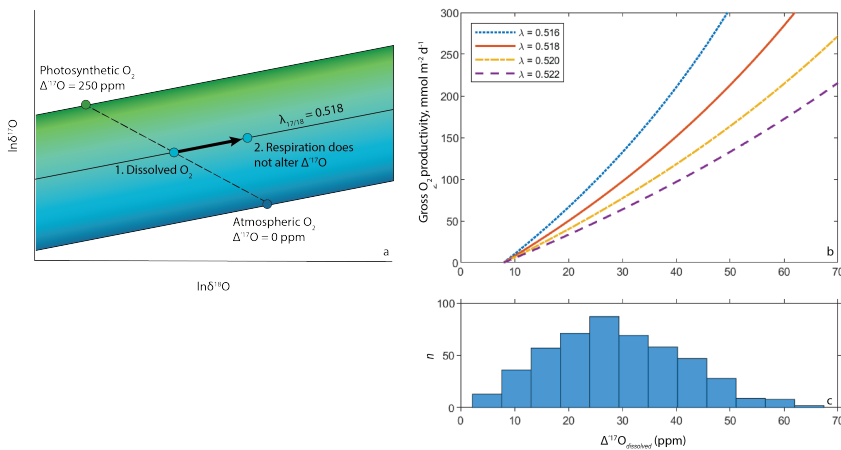
Figure 1: (a) Schematic (after Juranek and Quay)[21] showing how dissolved O_2 $\Delta'^{17}O$ can be a mixture of endmember atmospheric and photosynthetic O_2 compositions, and respiration fractionation that assumes $\lambda_{17/18}$ will preserve $\Delta'^{17}O$. (b) Calculated GOP plotted against $\Delta'^{17}O$ value for different λ values using the method of Prokopenko et al.[22] and photosynthetic O_2 from average marine phytoplankton according to Luz and Barkan[61] assuming $\delta'^{18}O_{O_2} = 0.73‰$, k = 3 m d^{-1}, and $[O_2]_{eq} = 230$ mol m^{-3}. (c) Histogram of $\Delta'^{17}O$ data from Reuer et al.[49]

Even small errors in the $\lambda_{17/18}$ and $\theta_{17/18}$ values for respiration have outsized consequences on triple-isotope-based calculations of GOP.[22, 58] As can be seen in Figure 1b-c, every 0.001 accuracy in $\lambda_{17/18}$ results in a 10-15% bias in GOP estimates; in the Southern Ocean, such errors could amount for up to 50 mmol O_2 m^{-2} d^{-1}.[49] While random analytical errors dominate the GOP uncertainty in low-productivity regions, systematic errors in $\lambda_{17/18}$ dominate GOP uncertainties in high-$\Delta'^{17}O$ regions.

θ values in multiply substituted isotopologues provide additional constraints

Measuring additional isotopologues, namely $^{17}O^{18}O$ and $^{18}O^{18}O$, reveals new covariations that can be used to constrain the uncertainty in $\theta_{17/18}$ values. We will use $^{18}O^{18}O$ (i.e., mass-36 O_2) in examples throughout; the reader is directed to earlier publications [28] for a thorough examination of other isotopologues.

Clumped-isotope geochemistry uses Δ_n notation in lieu of δ notation because it focuses on how isotopes are distributed among all possible isotopologues of a molecule.[62] The number of isotopologues containing more than one rare-isotope substitution is compared to that expected for a random (stochastic) distribution of isotopes.

(12)
$$\Delta_{36} = \left(\frac{^{36}R_{sample}}{^{36}R_{stochastic}} - 1 \right)$$

where

(13)
$$^{36}R_{stochastic} = \frac{\left[^{18}O \right]\left[^{18}O \right]}{\left[^{16}O \right]\left[^{16}O \right]} = \left(^{18}R \right)^2 \, .$$

This key difference between these definitions and similar-looking ones above (e.g., Eq. 1) is that the Δ_{36} value is explicitly normalized against the sample's $\delta^{18}O$ value. As written, then, Δ_{36} variations are independent of bulk isotopic composition and represent a new set of constraints on biogeochemical isotopic fractionation.

At this point it is useful to separate the processes that fractionate isotopologues into two broad categories: physical processes, which may move molecules but preserve their bonds, and chemical processes, which may alter, break, or make new bonds.

An example of a physical process that preserves bonds is diffusion. Knudsen diffusion, where gas flows through an orifice smaller than the mean free path of that gas, yields a calculable set of $\theta_{33/34}$, $\theta_{35/34}$ and $\theta_{36/34}$ values that can be compared directly to experiments [28]. The flux of gas

through the orifice is proportional to its velocity, and therefore inversely proportional to the square root of its mass. The relevant fractionation factor α can thus be predicted to be

$$(14) \qquad \alpha_{m_{36}} = \frac{^{36}R_{\text{diffused}}}{^{36}R_{\text{initial}}} = \sqrt{\frac{m_{32}}{m_{36}}}$$

where m is the molecular mass of the isotopologues. Similar to Eq. 8, isotopologue θ values can then be calculated as

$$(15) \qquad \theta_{36/34,\,diffusion} = \frac{\ln\left(\alpha_{36}\right)}{\ln(\alpha_{34})}$$

Solving eq. 15 for gas-phase O_2 self-diffusion yields $\theta_{33/34,\,diffusion} = 0.509$, $\theta_{35/34,\,diffusion} = 1.479$ and $\theta_{36/34,\,diffusion} = 1.943$; the subscripts indicate the cardinal mass of the species in the numerator and denominator of eq. 15, respectively. Note also that the subscript 34 here refers to $^{16}O^{18}O$, the main O_2 isotopologue at cardinal mass 34 and the primary contributor to the $\delta'^{18}O$ value of O_2.

The θ values derived from Knudsen diffusion experiments are generally in agreement with these calculated values, with a deviation of only 0.0008 observed for $\theta_{33/34,diffusion}$ likely associated with subtle experimental or instrumental artifacts.[27, 28] Studies of physical fractionation of O_2 due to gravitational settling and diffusion in water have yielded similar results, with $\theta_{33/34} < 0.52$, $\theta_{35/34} \leq 1.5$, and $\theta_{36/34} \leq 2.0$.[28, 63 29]

Chemical processes tend to fractionate over a different range of θ values. Here, we use an instructive example, the kinetically controlled breaking of an O-O bond. Equation 10 can be adapted to describe this process if (1) the fractionation is dominated by the atoms moving apart along the reaction coordinate and (2) isotope effects on activation energy are negligible. In that case, using the reduced masses of O_2, μ, instead of atomic masses in eq. 10 provides an

12

approximate description of the θ values.[33] To make this distinction clear, θ values will be denoted as θ_μ. Reduced masses are calculated as

$$(16) \qquad \mu = \frac{Mm}{M+m}$$

where M and m are the masses of the two atoms participating in the bond (e.g., both 17.99916 amu for $^{18}O^{18}O$). Therefore,

$$(17) \qquad \alpha_{36/34} = \sqrt{\frac{\mu_{32}}{\mu_{36}}} \ .$$

Solving eq. 15 for all O_2 isotopologues yields $\theta_{33/34,\mu} = 0.523$, $\theta_{35/34,\mu} = 1.553$ and $\theta_{36/34,\mu} = 2.061$. Unlike for physical fractionation, this example of chemical fractionation yields $\theta_{33/34} > 0.52$, $\theta_{35/34} \geq 1.5$, and $\theta_{36/34} \geq 2.0$.

While the examples within this section are somewhat generic, they nevertheless illustrate the differences in mass-dependent fractionation between physical and chemical mechanisms. These two broad categories of processes comprise those that can alter the isotopic composition of O_2 during respiration. Importantly, the contrasting ranges in θ have a qualitatively different effect on the Δ-values of the residual (i.e., not-yet-respired) O_2 pool: if respiration fractionation is controlled by physical processes, $\Delta'^{17}O$ ($\lambda_{17/18} = 0.518$), Δ_{35}, and Δ_{36} values will decrease in the residual O_2 pool. If respiration fractionation is controlled by chemical processes, then the quantities should increase.[28] First-principles calculations can be used to further constrain the expected range of θ values for each isotopologue pair.

Methods

Respiration experiments

Surface waters were sampled from Lake Houston's Deussen Park (29°55'7.1256" N, 95°8'56.9076" W) on June 15 and July 5, 2016 (hereafter referred to as LH1 and LH2) by casting a 20L Nalgene container from the dock and allowing it to fill with water. Upon retrieval, water was immediately partitioned into 300mL glass Wheaton bottles, stoppered and covered in aluminum foil to suppress light-dependent reactions in favor of dark respiration. Wheaton bottles were prepared for this experiment by acid washing in 50:50 HCl and 50:50 NaOH cold rinses, then autoclaved. Evacuated 2L flasks pre-poisoned with 400 μL of a saturated $HgCl_2$ solution were filled with ~400 mL of cast water, resulting in a final $HgCl_2$ concentration in excess of that recommended to halt respiratory activity in order to determine the starting conditions (t_0) of the following respiration experiment.[64]

Waters were transported to Rice University's Stable Isotope Lab for incubation at room temperature (measured as 25 ± 2°C); the time elapsed from first sampling at Lake Houston to lab was ~2 hours. Wheaton bottles were placed in a dark cabinet out of direct sunlight to limit temperature variations for the remainder of incubation (up to ~440 hours). One bottle was immediately unsealed and monitored with a calibrated Lazar Micro Oxygen Electrode to guide sampling throughout the experiment.

At intervals during the respiration experiment, Wheaton bottles were unsealed and water siphoned into pre-evacuated and poisoned 1L, 2L, and 5L flasks to halt respiration. The size of the flask was determined by the number of Wheaton bottles needed for combination to keep the final amount of O_2 to be analyzed between ~60-90 μmol and to keep the total volume of water less than half that of the flask. Filled flasks were transferred to an orbital shaker, where the dissolved O_2 equilibrated with the flask headspace for at least 48 hours before purification.

O_2 extraction, purification and mass spectrometry

Equilibrated flasks were inverted and the water was pumped through an evacuated flask until <1 mL water remained in the poisoned flask. At this point, the poisoned flask was isolated and moved to a vacuum line where the residual water was held at -40°C and headspace air was transferred, through two U-shaped traps held at -196°C (for drying), into a silica gel finger held at -196°C for 30-45 min.

Subsequent sample purification and mass spectrometry methods have been described previously.[27, 65] Briefly, the samples of dissolved air on silica gel fingers are moved to an automated gas-chromatograph (GC)-based O2 purification system. Gas samples are expanded off of the silica gel in a room-temperature water bath, cryogenically dried once more, then pre-concentrated onto a silica-filled U-trap prior to GC injection. Upon injection, the U-trap is heated to 90°C and flushed with helium for transfer to the GC column, which is held at -80°C to separate O2 from Ar and N2. Baseline resolution achieved by cryogenic separation of O2 and Ar permits each peak to be integrated (see Figure 2). Then, the ratio of these O2 and Ar peak areas are corrected for sample-size nonlinearity and compared to those in air to obtain δO2/Ar values:

$$
(18) \qquad \delta\left(\frac{O_2}{Ar}\right)_{air} = \left[\frac{\left(\dfrac{O_2}{Ar}\right)_{dissolved}}{\left(\dfrac{O_2}{Ar}\right)_{air}} - 1\right]
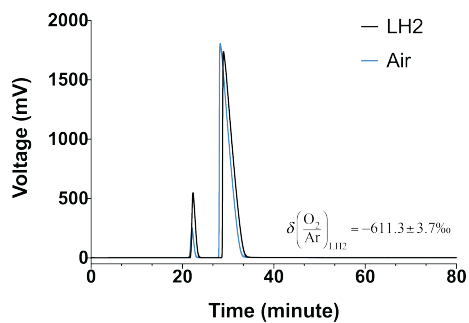$$

Figure 2: Typical chromatogram obtained from the thermal conductivity detector (25 mL min^{-1}, 1/8" x 3.05 m Molecular Sieve 5A column, 80/100 mesh) showing the baseline separation of O_2 and Ar (an important mass 36 interference) achieved during purification for both a standard air (blue line) and LH2 incubation (black line).

   These values are reported as per-mil deviations from air and show long-term reproducibility of ±4‰ (1σ). After the Ar is eluted, O_2 is recollected on a U-trap filled with silica gel and held at -196°C until the collection is finished and excess He is pumped out. Finally, O_2 is warmed to 90°C for 5 minutes prior to transfer to the isotope-ratio mass spectrometer (IRMS).

   After this final purification step, O_2 is transferred cryogenically to a cold prep finger adjacent to the mass spectrometer sample bellows for expansion and measurement relative to a laboratory working gas. The mass spectrometer used is a high-resolution Nu Instruments *Perspective IS* IRMS that typically achieves a mass resolving power (MRP) over 4000 where MRP $= m_{36}/(m_{95\%}-m_{5\%})$. This increase in MRP from prior methods resolves mass interferences that were known to be an issue such as Ar in addition to others that were not.[28] For example, $^{35}Cl^+$ (34.9689 amu) is resolved from $^{17}O^{18}O^+$ (34.9983 amu) on $m/z = 35$ and $^{36}Ar^+$ (35.9676 amu) as well as $H^{35}Cl^+$

(35.9767 amu) is resolved from $^{18}O^{18}O$ (35.9983 amu) on $m/z = 36$. Bulk isotopic compositions are reported relative to air-O_2, and clumped isotope distributions are reported relative to the stochastic distribution of isotopes and projected onto the theoretical reference frame.[66]

Sample compositions are calibrated by running them in sequence with a rotating set of standards such as O_2 generated from heating barium peroxide powder in sealed quartz tubes at 800°C, O_2 equilibrated by photolysis at a range of temperatures, as well as atmospheric O_2 and atmospheric O_2 dissolved in water.[28, 29, 63, 66] In addition, bulk isotope compositions are corrected for pressure-baseline effects that yield a triple-oxygen difference between atmospheric O_2 and San Carlos Olivine that has been reproduced across three independent labs within 10 ppm.[27, 30, 36, 67] This result implies that our measured $\lambda_{17/18}$ values are accurate to within 0.0006. Samples of atmospheric O_2 measured concurrently with respiration experiments (from June 2016-April 2017) had average values of $\delta^{18}O_{air} = 0.001 \pm 0.032‰$, $\Delta'^{17}O_{air, 0.518} = 0 \pm 4$ ppm, $\Delta_{36} = 1.992 \pm 0.042‰$ and $\Delta_{35} = 1.06 \pm 0.08‰$ (1σ, $n = 67$).[63]

Computational methods

Equilibrium isotope effects for chemical reactions can be calculated using reduced partition function ratios β for chemical species according to the formula

$$(19) \qquad \beta^* = \prod_i \left(\frac{v_i^*}{v_i} \right)_{MMI} \left(\frac{e^{-v_i^*/2}}{e^{-v_i/2}} \right)_{ZPE} \left(\frac{1-e^{-U_i}}{1-e^{-U_i^*}} \right)_{EXC} .^{41, 68}$$

In the oxygen system, the formula computes the isotopic fractionation relative to atomic O vapor. It can be conceptually split into three parts indicated by the subscripts: the classical mass- and moments-of-inertia (MMI) term, and the quantum-mechanical zero-point energy (ZPE) and excited-state (EXC) terms. The product comprising β is across all harmonic vibrational modes i.

The quantity $U_i = hc\nu_i/k_BT$ is the energy associated with any one vibrational mode, where h is Planck's constant, c is the speed of light, k_B is Boltzmann's constant, T is the temperature, and ν_i is the harmonic vibrational frequency in cm⁻¹. The asterisk denotes a heavy-isotope substitution. We have omitted the symmetry numbers in Eq. 20 because each isotopic species is considered explicitly in our calculations (see below).

First-principles calculations were performed on several analogues of biological heme-enzyme active sites. Density functional theory (DFT) was used to estimate the equilibrium isotopologue fractionation associated with reversible heme-O_2 binding at Cytochrome c oxidase (CcO) and other simplified oxyheme binding sites (Fig. 3). The reaction is treated as an isotope exchange reaction between free and bound O_2, i.e.,

(20) $$O_2^* + \text{heme} - O_2 \rightleftharpoons O_2 + \text{heme} - O_2^*$$
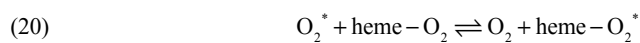
The calculations thus implemented simulate the isotopic effects of reversible O_2 binding with ferrous iron, a scheme exhibited by a number of important enzymes.[69, 70] The approach may be quantitative for θ values if distal electron-withdrawing moieties in enzymes have similar effects on equilibrium isotopologue effects.[71] Cytochrome c oxidase, for example, binds to O_2 in an end-on configuration with distal copper instead of the distal histidine residue found in hemoglobin, but the bonding scheme may be similar.[70, 72-76]

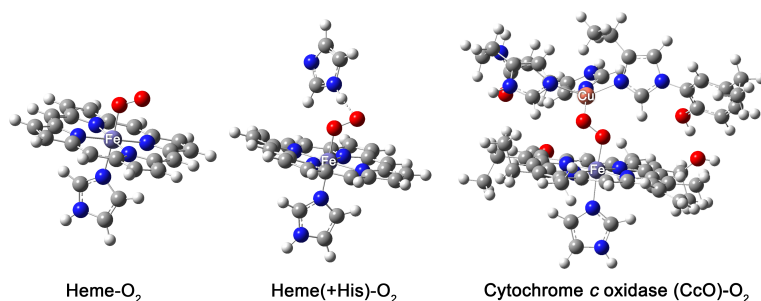Heme-O$_2$ Heme(+His)-O$_2$ Cytochrome *c* oxidase (CcO)-O$_2$

Figure 3. Oxyheme models used in this study. White atoms are hydrogen, grey atoms are carbon, blue atoms are nitrogen, and red atoms are oxygen. Transition-metal atoms (Fe, in lavender, and Cu, in orange) are labeled.

Three levels of theory were used to study heme-O$_2$ binding site models: (1) the Becke 3-parameter Lee-Yang-Parr functional using the D3 version of Grimme's empirical dispersion with Becke-Johnson damping (B3LYP-D3BJ),[77-79] (2) the one-parameter hybrid Tao-Perdew-Staroverov-Scuseria functional (TPSSh),[80, 81] and (3) the second-order generalized gradient approximation functional of Pervati, Zhao, and Truhlar (SOGGA11).[82] Each level of theory is paired with the Weigand-Ahlrichs split-valence Gaussian basis sets def2-SVP and def2-TZVP, which contain polarization functions and shows good accuracy for *d*-block elements.[83]

The first two functionals are global hybrid functionals, meaning that they treat the electron exchange-correlation energy in the Kohn-Sham DFT formulation by including a small amount of Hartree-Fock ("exact") exchange energy; B3LYP optimizes the exchange term using three parameters to yield ~20% exact exchange, while TPSSh uses one parameter to include 10% exact exchange. For metal-ligand systems, these semiempirical modifications compensate for the tendency of nonempirical functionals to bind ligands too strongly.[84] While B3LYP tends to bind

ligands to *d*-block elements too weakly[84], DFT studies of heme-O_2 systems suggest that empirical dispersion corrections can mitigate these shortcomings.[71, 85] In contrast, TPSSh was been found to be reasonably accurate in heme-O_2 systems without the need to invoke additional empirical corrections.[71, 86] The SOGGA11 functional is a pure, non-hybrid density functional based on the Perdew-Burke-Ernzerhof (PBE) functional hat has its exchange-correlation formulation optimized against a suite of molecular training sets for broad chemical applicability.[82, 87, 88]

For isotope fractionation calculations, the accuracy of harmonic vibrational frequencies is paramount. A recent assessment of optimal harmonic frequency scaling factors suggests that both the B3LYP method yields accurate frequencies without need for scaling.[89] The TPSSh functional has not been subject to such a study, but its scaling is likely intermediate between the TPSS (0% exact exchange, harmonic scaling factor 1.0194 when paired with def2-TZVP) and TPSS0 (25% exact exchange, harmonic scaling factor 0.9871 when paired with def2-TZVP basis) functionals.[89] Optimal frequency scaling factors for SOGGA11 paired with the def2-TZVP basis set have not been reported. For mass-dependent fractionation, cancellation of errors may limit errors related to methodological bias regardless of the nature of the frequency error.[90] The use of three DFT methods is a test of this assertion: one expects that the range in predicted single-isotope (i.e., $^{18}O/^{16}O$) fractionation will be larger than for multi-isotope/isotopologue trends because absolute harmonic frequency errors are cancelled during calculation of θ values. Anharmonic corrections were not included due to computational expense; previous work suggests they contribute ~0.001 errors in θ values.[91, 92]

Three molecular models were investigated: a neutral free oxyheme (Heme-O_2), a neutral oxyheme resembling that in hemoglobin [Heme(+His)-O_2], and O_2 bound to a simplified Cytochrome *c* oxidase active site (CcO-O_2; the **A** state of Chance et al.),[93] which has a +1 charge.

Calculations were performed in the Gaussian16 electronic structure program, revision B.01.[94] To simulate the effects of a solvent dielectric, a conductor-like polarizable continuum model (CPCM) for water (dielectric constant $\varepsilon = 78$) was used for Heme-O_2 and Heme(+His)-O_2 structures, while a CPCM with $\varepsilon = 4$ was used to simulate the CcO active site model being embedded within a supramolecular protein structure.[95] We note that while the choice of dielectric constant did not affect the results qualitatively, the inclusion of explicit waters near the binding sites could have an effect on calculated isotopic fractionations; effects on θ should be muted nevertheless. Geometries of all structures were first optimized using calculated analytical force constants, after which the frequencies calculated using the same level of theory and basis set. The presence of a stationary point was confirmed in all cases.

For Heme(+His-O_2), the distal histidine was represented as an imidazole and needed to be fixed in place relative to the porphyrin ring. As such, two calculations were performed: beginning with a previously published structure that was based on the O_2 binding site in human hemoglobin, a set of calculations—geometry optimization and frequency—was performed in which all 20 carbons in the porphyrin ring and 6 atoms of the distal imidazole were frozen (all three C atoms, the N atom, and two H atoms furthest from O_2).[75] Then, a second set of calculations was performed after "unfreezing" the 8 carbon atoms closest to the O_2 moiety and freezing only the nitrogen atom and the three distant hydrogen atoms of the distal imidazole. Because of these additional constraints, the first structure had 93 of 165 possible degrees of vibrational freedom (i.e., 56% of the total), whereas the second structure had 123 (75%). Both calculations yielded similar results, and only those for the latter, which has the least truncation of vibrational modes, are reported here. This approach resembles that employed by Rustad and coworkers to determine accurate isotopic fractionation factors from mineral clusters, wherein

atoms more than two bonds away from an isotopic substitution were assumed not to contribute significantly.[96, 97]

Equilibrium isotopologue fractionation between the heme-O_2 adduct and free (CPCM-dissolved) O_2 were calculated by inputting the computed harmonic frequencies of each molecule into eq. 20 to calculate harmonic β values. No frequency scaling was applied. The β values were used as constraints on O_2 isotopologue abundances for the bound species at equilibrium; isotopologue abundances satisfying a 9×9 array of β values (representing all possible combinations of O_2 + heme-O_2 isotopologues) were solved numerically using 8 parameters: $^{18}O/^{16}O$ and $^{17}O/^{16}O$ ratios, as well as Δ_{34} (for $^{17}O^{17}O$), Δ_{35}, and Δ_{36} values and 3 asymmetry parameters (one each for $^{16}O^{17}O$, $^{16}O^{18}O$, and $^{17}O^{18}O$) as inputs. Asymmetry parameters were included to account for the subtle isotopic preference for the heavy isotope to be bound to Fe in all cases e.g., Fe-$^{18}O^{16}O$ vs. Fe-$^{16}O^{18}O$. These parameters had a nominal value of 0.5, representing equal probabilities of binding between asymmetric O_2 isotopologues; typical fitted values are between 0.502 and 0.504, indicating a $0.5 - 1\%$ preference to bind the heavier isotope to Fe, which resulted in decreases in the magnitude of $^{18}\varepsilon$ of about 0.03‰ and increases in $\theta_{17/18}$, $\theta_{35/34}$ and $\theta_{36/34}$ of about 0.0008, 0.003, and 0.006, respectively.

Considering all known uncertainties together and exploiting the likely cancellation of errors associated with computing multi-isotopologue trends, we estimate that this approach yields $\theta_{17/18}$ values within ±0.001 of the true value for a given molecular model. Calculated $\theta_{35/34}$ and $\theta_{36/34}$ values may be less accurate, i.e., ±0.01.

Experimental results

Respiration rates

During the course of respiration studies, eleven standard air samples dissolved in water at 25°C were measured and found to have $\delta(O_2/Ar)_{air} = -92.0 \pm 2.5‰$ (95% CI), indistinguishable from the expected value of -91.9‰ at 25°C equilibrium.[29, 98, 99] For LH1 and LH2, $\delta O_2/Ar$ ratios at $t = 0$ are -185.4‰ and -312.0‰, respectively, and decrease linearly to -436.3‰ and -730.3‰ respectively (Figure 4, Table 1), equivalent to 0.45 µM h^{-1} and 0.27 µM h^{-1}, respectively.
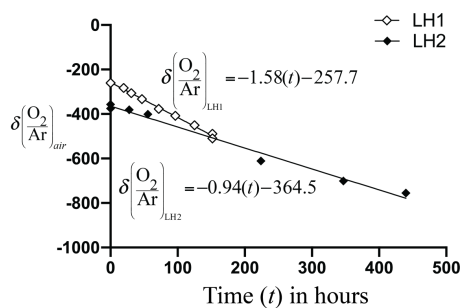
Figure 4. O$_2$/Ar ratios for LH1 and LH2 as a function of time. 1σ error bars from repeated measurements of air dissolved in water are smaller than symbols. Oxygen consumption rates are equivalent to 0.45 µM h^{-1} (LH1) and 0.27 µM h^{-1} (LH2).

Table 1. Isotopic compositions and O$_2$/Ar ratios for Lake Houston respiration

Experiment	Time (hours)	$\delta(O_2/Ar)_{air}$ / ‰	f	$\delta^{18}O$ / ‰	$\Delta'^{17}O*$ / ppm	Δ_{35} / ‰	Δ_{36} / ‰
LH1	0†	-260.7	1.0	-0.17	35	0.94	1.77
LH1	19.67	-282.7	0.97	0.68	52	1.12	1.86
LH1	30.92	-306.4	0.94	1.43	53	0.98	1.81

LH1	46.9	-332.7	0.90	1.81	56	0.97	1.88
LH1	71.8	-377.2	0.84	3.11	71	1.09	1.87
LH1	96.42	-408.1	0.80	4.31	68	1.00	1.96
LH1	125.17	-450.0	0.74	6.46	81	1.02	1.92
LH1	151.67	-488.4	0.69	7.26	85	0.97	1.94
LH1	151.67	-509.4	0.69	7.48	75	0.93	1.99
LH2	0†	-375.6	1.0	0.47	28	1.03	1.95
LH2	0†	-356.9	1.03	0.36	26	0.97	1.88
LH2	27.9	-381.0	0.99	1.46	36	0.95	1.92
LH2	55.7	-401.0	0.96	2.46	34	1.04	1.95
LH2	223.9	-611.3	0.62	12.55	91	1.24	2.25
LH2	346.8	-701.2	0.48	17.35	128	1.41	2.39
LH2	439.8	-755.2	0.39	20.95	109	1.27	2.58

Errors are 1σ calculated from 11 repeated measurements of air equilibrated in water at 25°C, and correspond to ±3.7‰, ±0.05‰, ±4 ppm, ±0.09‰, and ±0.03‰ for $\delta(O_2/Ar)_{air}$, $\delta^{18}O$, $\Delta'^{17}O$, Δ_{35}, and Δ_{36}, respectively.

*λ=0.518

†Sampled directly from Nalgene into poisoned bottle; not used in calculations of α and θ.

Bulk and clumped isotope variations for Lake Houston respiration

Values of $\delta^{18}O$, $\Delta'^{17}O$, Δ_{35} and Δ_{36} for LH1 and LH2 are listed in Table 1 and shown varying with time in Figure 5. During the course of LH1 and LH2, 31% and 61% of the initial O_2 concentrations were consumed, respectively. All isotopic indices in the residual O_2 ($\delta^{18}O$, $\Delta'^{17}O$, Δ_{35}, and Δ_{36}) tended to increase over the course of the experiments. At t = 0, $\delta^{18}O$ values are -0.17‰ and 0.47‰ for LH1 and LH2 respectively, and they increase linearly to 6.46‰ and 20.95‰ respectively (Figure 5a). $\Delta'^{17}O$ values increase from 35 ppm to 81 ppm and from and

28 ppm to 109 ppm for LH1 and LH2, respectively (Figure 5b). During LH1, average Δ_{35} value

is $1.01 \pm 0.06‰$ (1σ) with no discernable trend through time. However, Δ_{35} values during LH2

increase from $1.03‰$ to $1.3‰$ (Figure 5c). Values of Δ_{36} increase from $1.77‰$ to $1.92‰$ for

LH1 and from $1.95‰$ to $2.58‰$ for LH2 (Figure 5d).

Qualitatively, these results are consistent with those associated with respiration during a

previous multi-phase terrarium experiment.[57] The previously observed "anomalous" covariation

of Δ_{35} and Δ_{36} values is not observed: Δ_{35} values increase about half as much as Δ_{36} values
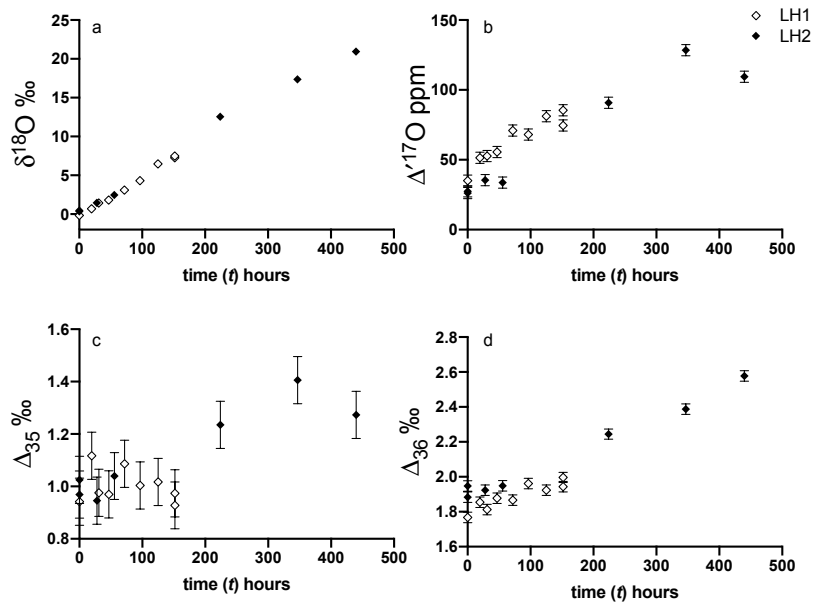
during experiment LH2, where such trends would be clearly visible.

Figure 5. Variations in $\delta^{18}O$, $\Delta'^{17}O$, Δ_{35} and Δ_{36} for LH1 (white diamonds) and LH2 (black diamonds) as a function of time. Error bars are 1σ from replicate measurements of air dissolved in water and are smaller than symbols for $\delta^{18}O$.

Calculation of experimental α, $\theta_{17/18}$, $\theta_{36/34}$, and $\theta_{35/34}$ values

The evolution of isotopes in these respiration experiments can be described by closed-system Rayleigh fractionation if each incubation bottle had the same starting composition and microbial community. We derive effective isotopologue fractionation factors α relative to $^{16}O^{16}O$ by regressing $\ln(R/R_0)$ vs. $\ln f$ to obtain $\alpha - 1$, where f is the proportion of initial O_2 remaining in the sample (Figure 6a) determined by assuming that $\delta O_2/Ar_{t=0}$ is 100% of the O_2.

$$(21) \qquad \ln\left(\frac{^{36}R}{^{36}R_0}\right) = \left(^{36}\alpha_{resp} - 1\right) \cdot \ln(f)$$

θ_{resp} values were obtained using the relevant variants of Eq. 15. Uncertainties in $^{18}\alpha$ values were computed from the linear regressions assuming the uncertainty in f is insignificant compared that in $\delta'^{18}O$, using the same nominal uncertainties for all points. Uncertainties in θ values were propagated from fit uncertainties in cross-plots of δ' values, which yield slopes related to θ values (Figure 6b). These slopes also implicitly normalize for error covariance in α values through the relation:

$$(22) \qquad slope = \left(\frac{1-\alpha^\theta}{1-\alpha}\right) \qquad\qquad (23)$$

Resulting values for $^{18}\alpha_{resp}$ are 0.9809 ± 0.0010 and 0.9791 ± 0.0008 (1σ) for LH1 and LH2, respectively, and the corresponding $^{18}\varepsilon$ values are $-19.1 \pm 1.0\text{‰}$ and $-20.9 \pm 0.8\text{‰}$ (1σ)

respectively. When LH1 and LH2 are averaged together, the implied θ_{resp} values are $\theta_{33/34,\,resp}=$ 0.5200 ± 0.0001, $\theta_{35/34,\,resp} = 1.53 \pm 0.02$, and $\theta_{36/34,\,resp} = 2.05 \pm 0.01$ (1σ). All θ_{resp} values and their associated best-fit uncertainties are listed in Table 2.
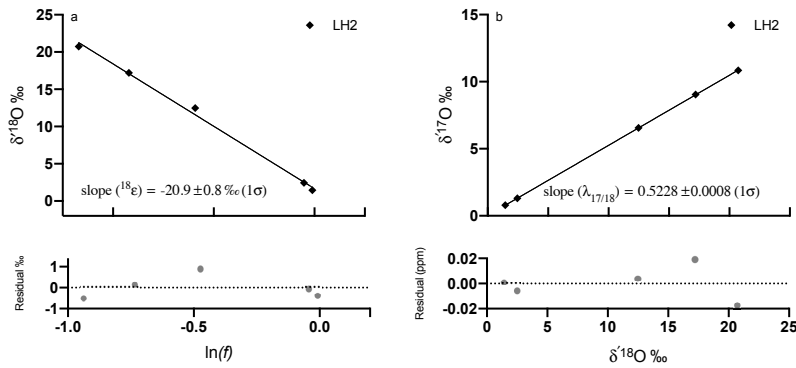

Figure 6. LH2 data are shown as a representative example of the evolution of $\delta'^{18}O$ vs. the natural log of the fraction of O_2 remaining (a). The linear regression slope of this line is $^{18}\varepsilon$. Panel (b) shows the co-variation in $\delta'^{17}O$ vs $\delta'^{18}O$, and the linear regression slope of this line is $\lambda_{17/18}$. Residuals for these regressions are shown in the bottom of each panel.

The results are robust: removing any one data point from each time trace yields best-fit $^{18}\alpha_{resp}$ and θ_{resp} values within the stated uncertainty limits. Because these experiments may not have sampled identical microbial communities, some heterogeneity is expected with respect to both initial state and effective fractionation factors. However, the large water volumes required for analysis seem to limit such effects.

27

Table 2. Measured θ_{resp} for LH1 and LH2

i/j	θ_{resp} LH1	1σ	θ_{resp} LH2	1σ
17/18	0.5200	0.0007	0.5201	0.0009
35/34	1.517	0.009	1.551	0.006
36/34	2.040	0.005	2.055	0.002

Computational results

Bond lengths and harmonic vibrational frequencies (ν) of key bonds in the oxyhemes studied (Fig. 3) are listed in Table 3. All methods reproduced the experimental O-O bond length in O_2 within several picometers. All heme-O_2 adduct structures were open-shell singlets (^1A symmetry), with antiparallel spin densities on Fe and O_2 and partial negative charges on O_2, consistent with experimental inferences and previous computational studies.[72, 74, 75] Calculated O-O and Fe-O bond lengths in the oxyhemes were generally close to experimental values, although B3LYP-D3BJ and TPSSh methods show longer Fe-O and O-O bonds. All methods reveal an extension of the O-O bond length upon binding, indicating a reduction in bond order associated with an increase in local charge density. We note that the results reported for CcO-O_2 correspond to calculations using the smaller def2-SVP basis set (as opposed to def2-TZVP), because the large system size greatly increased computational expense. Calculations on the other models using def2-SVP basis yielded slightly different results, but differences in $\theta_{17/18}$ values were typically $O(10^{-4})$, while differences in $\theta_{35/34}$ and $\theta_{36/34}$ values were <0.01 except for SOGGA11, which generally showed the largest variability in results.

Some spin contamination was identified in the hybrid DFT wavefunctions (likely arising from Hartree-Fock exchange), but previous work on oxygenated metalloprotein analogues suggests

28

that such has little effect on the optimized geometries.[100] Bond lengths derived from the

SOGGA11 functional (which lacks exact exchange) showed better agreement with experimental

crystal structures, but solvated structures appear to be in better agreement with the TPSSh and

B3LYP-D3BJ structures.[101] A full investigation of the accuracy of these methods is beyond the

scope of this work in part because the associated errors seem to largely cancel when θ values are

computed (see below).

Table 3. Key bond lengths and vibrational frequencies for optimized oxyheme structures

Structure/Basis	Method	Bond	Length (Å)	ν (cm^{-1})	Reference
O_2	B3LYP-D3BJ	O-O	1.204	1637	
def2-TZVP	TPSSh	O-O	1.208	1618	
	SOGGA11	O-O	1.210	1577	
	Experiment	O-O	1.207	1580	[102]
Heme-O_2	B3LYP-D3BJ	O-O	1.296	1223	
def2-TZVP	TPSSh	O-O	1.296	1204	
	SOGGA11	O-O	1.274	1231	
	B3LYP-D3BJ	Fe-O	1.878	533	
	TPSSh	Fe-O	1.863	536	
	SOGGA11	Fe-O	1.801	517	
Heme(+His)-O_2	B3LYP-D3BJ	O-O	1.302	1218	
def2-TZVP	TPSSh	O-O	1.304	1190	
	SOGGA11	O-O	1.283	1201	
	Experiment (HbO$_2$)	O-O	1.32-1.34	1155	[101, 103, 104]
	B3LYP-D3BJ	Fe-O	1.877	527	
	TPSSh	Fe-O	1.857	530	

	SOGGA11	Fe-O	1.794	458	
	Experiment (HbO$_2$)	Fe-O	1.83	568	[101, 104]
CcO-O$_2$	B3LYP-D3BJ	O-O	1.384	952	
def2-SVP	TPSSh	O-O	1.368	936	
	SOGGA11	O-O	1.295	1142	
	B3LYP-D3BJ	Fe-O	1.827	584	
	TPSSh	Fe-O	1.819	583	
	SOGGA11	Fe-O	1.814	544	
	Experiment (CcO)	Fe-O		571	[105]

The harmonic ^{16}O-^{16}O stretching frequencies for free O$_2$ calculated by SOGGA11 (e.g., 1577 cm^{-1} for CPCM-solvated O$_2$) showed the best agreement with experiment (e.g., 1580 cm^{-1} for O$_2$ gas [102]), followed by TPSSh and then B3LYP-D3BJ. We note that O$_2$ dissolution is associated with a frequency shift of ~9 cm^{-1}, which is not captured in these calculations.[106] Nevertheless, the resulting fractionation is small, contributing errors of <1‰ in $^{18}\varepsilon$ and negligible errors in θ values. [29, 98] The best point of comparison for ^{16}O-^{16}O stretching frequencies in the oxyhemes (given a lack of experimental data) is between Heme(+His)-O$_2$ and oxyhemoglobin, which have vibrational frequencies of ~1200 cm^{-1} and 1155 cm^{-1} respectively.[103] We consider these to be in good agreement considering that the observed vibrational frequency includes anharmonic effects. The ^{16}O-^{16}O stretching frequencies in CcO-O$_2$ have not been directly observed, so their accuracy is not known. Harmonic Fe-^{16}O stretching frequencies were similar between TPSSh and B3LYP-D3BJ levels of theory [~530 cm^{-1} for $^{16}O^{16}O$ bound in in Heme-O$_2$ and Heme(+His)-O$_2$, and ~583 cm^{-1} for CcO-O$_2$], and significantly lower for SOGGA11. We note that the TPSSh and B3LYP-

D3BJ Fe-O stretching frequencies are similar to experimental values determined by resonance
Raman techniques.[104, 105]

Calculated isotopologue fractionations between 5°C and 50°C are shown in Fig. 7, and values
at 25°C are listed in Table 4. All $^{18}\varepsilon$ values are predicted to increase in magnitude with
increasing temperature, although the total change over the temperature range is less than 1‰.
Results from calculations utilizing the def2-SVP basis set yielded $^{18}\varepsilon$ values of 1-2‰ larger
magnitude. Calculated $^{18}\varepsilon$ values show only minor differences between TPSSh and B3LYP-
D3BJ methods. The SOGGA11 method yielded much weaker $^{18}O/^{16}O$ fractionation than the other
methods for Heme-O_2 and CcO-O_2. The $^{18}\varepsilon$ values for the oxyhemoglobin analogue Heme(+His)-
O_2 are larger in magnitude than those determined by experiments on human subjects and horse-
heart hemoglobin, i.e., -8.0‰ vs. -4‰ to -6‰ at 25°C.[9, 44, 107] Systematic error in the calculations
may arise from inaccuracy in the β values for dissolved O_2, stemming from errors in both the O_2
and solvent vibrational frequencies. Indeed, using $\omega_e = 1580$ cm^{-1} for dissolved O_2 resolves the
discrepancy between theoretical and experimental $^{18}\varepsilon$ values for oxyhemoglobin. However,
systematic errors in DFT methods lead to a wide range of errors in ν (e.g., Fe-^{16}O frequency is
lower than experiment, while O-O frequency is higher), so tying ν for O_2 to the experimental
result may not be justified.

Table 4. Calculated equilibrium isotopic fractionation factors for heme-O_2 at 25°C

Structure/Basis	Method	$^{18}\varepsilon$ (‰)	$\theta_{17/18}$	$\theta_{35/34}$	$\theta_{36/34}$
Heme-O_2	B3LYP-D3BJ	-9.1	0.525	1.581	2.107
def2-TZVP	TPSSh	-8.9	0.525	1.582	2.109
	SOGGA11	-5.5	0.524	1.603	2.151

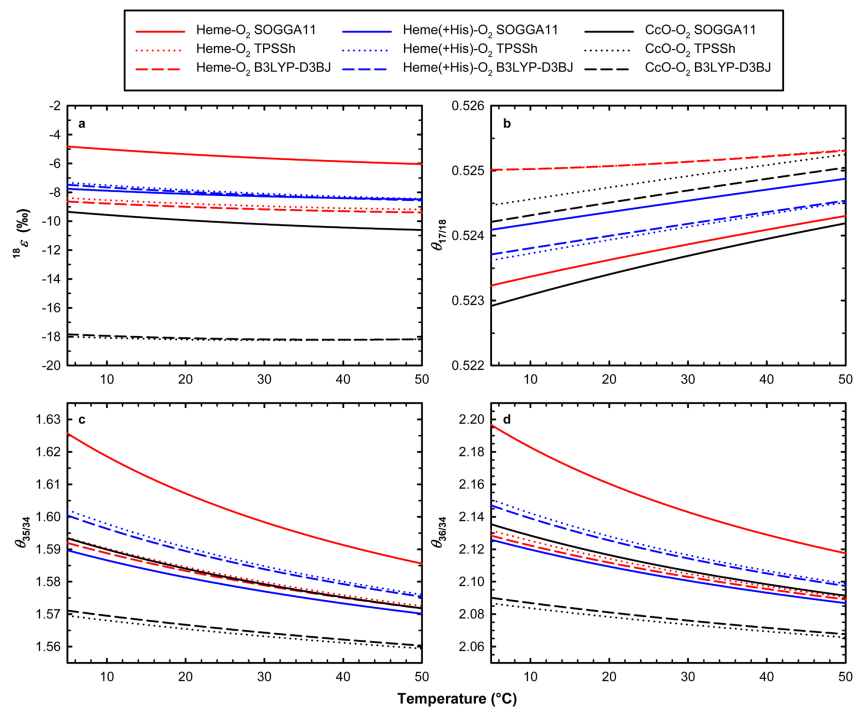|						
Heme(+His)-O$_2$	B3LYP-D3BJ	-8.1	0.524	1.587	2.120
def2-TZVP	TPSSh	-8.0	0.524	1.588	2.122
	SOGGA11	-8.2	0.524	1.579	2.105
CcO-O$_2$	B3LYP-D3BJ	-18.2	0.525	1.565	2.078
def2-SVP	TPSSh	-18.2	0.525	1.564	2.076
	SOGGA11	-10.1	0.524	1.582	2.111

Figure 7. Calculated equilibrium isotopologue fractionation for heme-O$_2$ structures. Shown

are (a) $^{18}O/^{16}O$ fractionation as $^{18}\varepsilon = {}^{18}\alpha - 1$, (b) $\theta_{17/18}$, (c) $\theta_{35/34}$, and (d) $\theta_{36/34}$ values for the three

model oxyheme structures. Heme-O_2 and Heme(+His)-O_2 results are obtained using the def2-TZVP basis set, while for CcO-O_2 they are obtained using the def2-SVP basis set.

The $\theta_{17/18}$ values for equilibrium fractionation are nearly identical between heme-O_2 adduct structures: all $\theta_{17/18}$ values are within 0.001 of 0.524 at 25°C, independent of both theory and basis set size. They show a subtle increase (<0.001) predicted over the temperature range. The nearly negligible variation between levels of theory and basis suggests that these results are robust for these molecular models, perhaps due to a cancellation of errors in Eq. 18. Calculated $\theta_{35/34}$ and $\theta_{36/34}$ values are more variable, although $\theta_{35/34} > 1.5$ and $\theta_{36/34} > 2.0$ in all cases. $\theta_{35/34}$ and $\theta_{36/34}$ values also show a slightly larger temperature dependence than $\theta_{17/18}$ values. The progressive decrease in $\theta_{35/34}$ and $\theta_{36/34}$ values from Heme-O_2 → Heme(+His)-O_2 → CcO-O_2 may be related to the strength of the heme-O_2 interaction or the redistribution of rotational degrees of freedom as the O_2 experiences stronger interactions with distal moieties in the bound state. Again, SOGGA11 shows the largest deviations from other levels of theory, perhaps due to the aforementioned tendency of nonempirical functionals to overbind ligands.[84]

Discussion

Comparison of new laboratory experiments with previous results

Both of our incubations of natural waters yielded effective $\theta_{17/18,resp}$ values of 0.520, which is higher than the range of values (0.510 – 0.515) reported for dark respiration. [26, 44] Possible origins of these discrepancies are diverse.

One potential source of the discrepancy is pathway-specific differences in oxygen consumption. In natural waters, respiration no doubt progresses through a combination of mechanisms, even when incubated in the dark. However, an incubation of natural waters from Lake Kinneret [44] yielded a $^{18}\varepsilon$ value indistinguishable from what we observed (-21.6 ± 0.1‰ vs. -

20.0 ± 1.3‰, 1σ) and a $\theta_{17/18,resp}$ value indistinguishable from those later obtained for pathway-specific experiments analyzed in the same lab.[12, 44] Diffusion in water has $^{18}\varepsilon \approx$ -3.3‰ and $\theta_{17/18} =$ 0.517 ± 0.002 (1σ), so diffusion control is unlikely in our experiments and cannot have driven $\theta_{17/18,resp}$ to higher values.[29, 108] Light-dependent O_2 consumption mechanisms may have higher $\theta_{17/18}$ values, but the absence of light in these experiments inhibited their expression.[3, 4] In addition, O_2 isotope-exchange reactions on metal oxide surfaces are likely too slow at 25°C to for them to have affected the isotopic composition of dissolved O_2 in our experiments.[109] Indeed, the observation of Δ_{36} values increasing above their 25°C-equilibrium composition in both experiments (e.g., by 1‰ in LH2) argues against significant oxygen isotope exchange. Finally, air contamination in latter samples would tend to lower measured $\theta_{17/18}$ values. Therefore, we consider our incubation experiments representative of dark respiration fractionation in natural freshwater, with little, if any, expression of known "high-$\theta_{17/18}$" pathways that would artifactually increase $\theta_{17/18,resp}$ by ≥0.004.

A second potential source of the discrepancy is the difference in analytical method. Unlike other labs, we analyze pure O_2 without Ar, and our measurements are calibrated against multiple standards that together show good agreement in triple-oxygen composition relative to two other high-precision labs utilizing identical sample preparation methods.[27] Laboratories that do not separate O_2 from Ar must empirically correct for the presence of Ar using calibrated O_2/Ar mixtures. We have shown recently that varying amounts of isobaric interferences can render triple-isotope measurements inaccurate: undesired isobars that scatter onto the O_2 analyte masses in a mass spectrometer can exacerbate "pressure baseline" scale distortion effects, which tend to decrease measured $\theta_{17/18}$ values relative to their true values. Errors in $\theta_{17/18}$ of 0.005 were shown to be possible using a realistic range of isobaric signals.[27] Whether these errors were present in

previous experiments is not known, but our reported measurements include explicit corrections for these effects.

Regardless of the reason for the $\theta_{17/18,resp}$ discrepancy between labs and experiments, a discussion of theoretical context of all θ_{resp} values ($\theta_{17/18,resp}$, $\theta_{35/34,resp}$, and $\theta_{36/34,resp}$) is warranted to examine whether reported θ_{resp} values are consistent with conceptual models for respiratory isotopologue fractionation. The novel determination of $\theta_{36/34,resp}$ and $\theta_{35/34,resp}$ values for dark respiration in this study provides additional constraints on these conceptual models and the associated $\theta_{17/18,resp}$ value(s) expected.

Understanding natural variability in θ values in simplified cases

In this section, we will explore how processes governed by the mass of O_2 molecules or the mass of oxygen atoms participating in O-O bonds may influence mass-dependent fractionation during respiration. Our goal is to understand the mechanistic origins of the θ_{resp} values observed in Lake Houston waters. We will restrict our discussion to θ values because they appear to be less variable than α values for respiration, both in our experiments and in the literature.[3, 12, 44] Theoretical reasons for the relative invariance in θ values among different processes have been reviewed elsewhere.[32, 33]

Diffusive fractionation (Table 5, Rows C. D, and E) is likely relevant for respiration because O_2 must travel from the lipid membrane (where it is several times more soluble than in the surrounding medium)[110] to the respiratory enzyme. Moreover, O_2 may also need to diffuse through protein channels toward the active site (in Cytochrome c oxidase, for example).[72] If O_2-containing water clusters are the relevant diffusing unit (e.g., whole clusters diffusing amongst themselves), then one can use the total masses of the isotopically substituted clusters in eq. 14, and calculate θ values via eq. 15 (Table 5, Row D). If O_2 itself diffuses through the medium

rather than a larger cluster, then the process is represented using the reduced mass of O_2 and its average diffusive partner instead (Table 5, Row E). Regardless of the specific diffusive mechanism, neither of these scenarios alone are sufficient to describe the empirically determined θ_{resp} values; they are all too low, and would drive $\Delta'^{17}O$, Δ_{35}, and Δ_{36} values down over the course of the experiment, contrary to what is observed (Fig. 5).

Table 5. Calculated and measured θ values describing physical and chemical fractionation mechanisms potentially relevant for respiration in natural waters

		$\theta_{17/18}$	$\theta_{33/34}$	$\theta_{35/34}$	$\theta_{36/34}$	Equation	Relevant mechanism
A[†]	$\theta_{kin,\ atomic}$	0.516	0.516	1.516	2.000	10	-
B	$\theta_{eq,\ high\text{-}temperature\ limit}$	-	0.531	1.531	2.000	11	-
C	$\theta_{m,\ gas\text{-}phase\ self\text{-}diffusion}$	-	0.509	1.479	1.943	15	-
D	$\theta_{m,\ diffusion\ with\ water}$	-	0.504	1.493	1.977	15*	O_2 traveling to the respiration site within a water cluster
E	$\theta_{\mu,,\ interdiffusion}$	-	0.515	1.461	1.897	15&	O_2 diffusing to the active site through water
F	$\theta_{\mu,O2}$	-	0.523	1.555	2.061	15	Kinetically controlled O_2 bond breaking for free O_2
G	$\theta_{\mu,,O2\text{-}M}$	-	0.524	1.552	2.053	15%	Kinetically controlled O_2 bond breaking for O_2 bound to ^{56}Fe
H	$\theta_{CcO,bind}$	-	0.525	1.564	2.076		Equilibrium O_2 binding to model CcO
I	$\theta_{resp\ LH1}$	0.520	0.520	1.517	2.040	-	-
J	$\theta_{resp\ LH2}$	0.520	0.520	1.551	2.055	-	-

Atomic masses used in these calculations are 15.99491 amu, 16.99913 amu, and 17.99916 amu for ^{16}O, ^{17}O, and ^{18}O, respectively.

[†]Isotopologue θ values correspond to purely statistical fractionation for the given $\theta_{17/18}$.

*For an O_2 molecule traveling along with 3 water molecules, each with a mass of 18.0156. Ranges for 1 to 10^7 water molecules are 0.506/1.487/1.962 – 0.501/1.501/1.999 for $\theta_{33/34}$/ $\theta_{35/34}$/ $\theta_{36/34}$ respectively.

&For an O_2 molecule interdiffusing through clusters of 3 water molecules, each with a mass of 18.0156. Ranges for 1 - 10^7 water molecules are 0.514/1.465/1.907 – 0.516/1.458/1.889 for $\theta_{33/34}$/ $\theta_{35/34}$/ $\theta_{36/34}$ respectively.
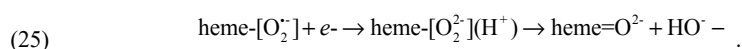
%For an O_2 molecule interacting with a single particle of mass 56. Ranges for particles of mass 1-10^7 are 0.530/1.533/2.006 – 0.523/1.555/2.061 for $\theta_{33/34}$/ $\theta_{35/34}$/ $\theta_{36/34}$ respectively. Holding mass 56 constant, the ranges in θ values for the number of particles from $1 - 10^7$ are 0.524/1.552/2.052 – 0.531/1.531/2.000.

Chemical fractionation, achieved through the alteration or rupture of the O-O bond of O_2, plays a role in determining θ_{resp} values as well. Using Eqs. 15 and 17, we can calculate θ values for kinetically controlled O-O bond breaking in a free O_2 molecule and for O_2 bound to ^{56}Fe [where $(1/\mu) = \Sigma(1/m)$ for ^{56}Fe-O_2]. These computed θ values, along with the results of DFT calculations on oxyheme models, are qualitatively consistent with the experimental θ_{resp} values, i.e., they would drive $\Delta'^{17}O$, Δ_{35}, and Δ_{36} values up over the course of the experiment, although there are quantitative disagreements in detail: the predicted $\theta_{17/18}$, $\theta_{35/34}$, and $\theta_{36/34}$ values are all slightly larger than our experimental values.

Some combination of physical and chemical fractionations, dominated by chemical fractionation, may thus explain our laboratory data ($\theta_{17/18} = 0.520$, $\theta_{35/34} = 1.53$ and $\theta_{36/34} = 2.05$, on average). In contrast, the discrepant laboratory data from other labs—if no systematic analytical errors are present—require a larger, if not dominant contribution from physical effects. We will examine the plausibility of this scheme with a more detailed mechanistic analysis of biological O_2 consumption below.

The role of electron-transfer processes for respiratory O_2 fractionation

Aerobic respiration is often viewed simplistically through the lens of kinetic mass-dependent fractionation of oxygen isotopes (e.g., eq. 10), but the view is conceptually flawed: O-O bond-breaking at respiratory enzymes requires the transfer of two electrons (out of four total for O_2 reduction to water), each of which weakens the O-O bond. In Cytochrome *c* oxidase, it occurs in two distinct steps that are shown schematically below:[72, 111]

(24)
$$O_2 + heme \rightleftharpoons heme\text{-}[O_2^{\cdot-}]$$

(25)
$$heme\text{-}[O_2^{\cdot-}] + e\text{-} \rightarrow heme\text{-}[O_2^{2-}](H^+) \rightarrow heme\text{=}O^{2-} + HO^- -$$.

The first elementary step involves electron transfer from the proximal heme to O_2; it is reversible, so may exhibit equilibrium fractionation described by isotope-exchange reaction 21.[112] The second step is coupled with proton transfer.[74, 111] Previous studies suggest it may be irreversible in many respiratory oxidoreductases, serving to "commit" the enzyme to O_2 reduction.[113] Importantly, each electron, when added to O_2, weakens the bond, resulting in a reduced force constant and a lower O-O vibrational frequency. Our calculations on the first of these steps, heme-O_2 binding, reveal high θ values consistent with chemical fractionation as described in the preceding section, i.e., $\theta_{17/18} \approx 0.525$, $\theta_{35/34} \approx 1.56$, and $\theta_{36/34} \approx 2.08$ at 25°C in the CcO-O_2 model for the TPSSh and B3LYP-D3BJ methods. While few mechanisms of the diverse oxidoreductases that operate in nature have been elucidated, both the cytochrome and cyanide-resistant alternative oxidase pathways appear to elongate the O-O bond during binding, either in an end-on or side-on geometry.[114, 115] This mechanism may explain the invariance of $\theta_{17/18,resp}$ previously observed for a range of respiratory pathways.[44]

As others have noted, the reduction in bond order during heme-O_2 binding resembles that between O_2 and $O_2^{\cdot-}$ (superoxide anion).[72, 107] Indeed, the charge-transfer equilibrium between O_2 and O_2^- yields an isotopologue mass dependence similar to that calculated for the oxyhemes: using vibrational frequencies of 1580 cm^{-1} and 1175 cm^{-1} for $^{16}O^{16}O$ and $^{16}O^{16}O^-$, respectively, and evaluating the equilibrium isotopologue fractionation in the reaction $O_2^* + O_2^- \rightleftharpoons O_2 + O_2^{-*}$,

38

we obtain $\theta_{17/18} = 0.527$, $\theta_{35/34} = 1.541$, and $\theta_{36/34} = 2.027$ at 25°C.[102, 116] The differences between this simple case and that of the oxyhemes may be attributed to the specific nature of the heme-O_2 electron transfer and/or reduction in symmetry in the heme-[$O_2^{\cdot-}$] adduct compared to free O_2^-. Small deviations in these vibrational frequencies (up to tens of cm^{-1}) do not alter the basic observations for θ values reported here.

The second electron transfer step, reaction 26, is not well understood. It is likely kinetically controlled, but the relevant transition-state structure is poorly known, preventing a confident DFT-based estimate of its kinetic isotopologue fractionation to be made at present.[74, 111] Nevertheless, one can examine proton-transfer and electron-transfer limitation qualitatively. For the former case, formation of an O-H$^+$ bond is limiting; because the reaction coordinate involves bonds other than the O-O bond, the mass dependence of the reaction may lie somewhere between θ_{kin} and θ_μ values in Rows A and F of Table 5.[32] For electron-transfer limitation, motion along the reaction coordinate dominates, so the reaction's mass dependence may resemble θ_μ values in Rows F and G of Table 5.

Both electron-transfer steps yield predicted θ values that are qualitatively consistent with our experimental results across all isotopologues, i.e., $\theta_{17/18} > 0.516$, $\theta_{35/34} > 1.5$, and $\theta_{36/34} > 2.0$ at 25°C. These θ values would generally yield an increase $\Delta'^{17}O$, Δ_{35}, and Δ_{36} values in the residual O_2. Our experimental data are thus consistent with the expectation that respiratory fractionation is strongly controlled by chemical factors. This interpretation is inconsistent with the results from other laboratories, however, which would require a larger contribution from physical fractionation to explain their $\theta_{17/18}$ values.

Two-step model for isotopic fractionation at a respiratory oxidase

To quantify how these chemical- and diffusion-dominated models differ, and to determine whether the clumped-isotope data can distinguish between them, we utilized the two-step enzyme fractionation model from Stolper et al. (2018) based on the reaction sequence

(26) $$O_2(\text{free}) \rightleftharpoons O_2(\text{active site}) \rightarrow \text{products}$$
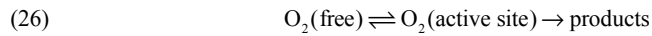
The first step represents O_2 diffusing to the enzyme active site. The second step encompasses both the O_2 binding and reduction steps. We chose to combine the two latter steps for this exercise because they show a similar range of θ values. Our goal is to use the model to distinguish between diffusive and electron-transfer limitation of respiratory O_2 consumption. For this reaction sequence, the measured isotopic fractionation factors (α_{measured}) can be described using fractionation factors for aqueous diffusion and enzymatic reduction ($\alpha_{\text{diffusion}}$ and α_{enzyme}, respectively) and a reversibility parameter r ranging from 0 to 1, where $r = 1$ indicates complete reversibility in the first step, i.e., no diffusive fractionation:

(27) $$\alpha_{\text{measured}} = \frac{\alpha_{\text{diffusion}}}{r\left(\dfrac{\alpha_{\text{diffusion}}}{\alpha_{\text{enzyme}}}\right) + 1 - r}$$

For diffusive fractionation, we use $^{18}\varepsilon_{\text{diffusion}} = -3.3‰$, $\theta_{17/18,\,\text{diffusion}} = 0.5146$, $\theta_{35/34,\,\text{diffusion}} = 1.462$, and $\theta_{36/34,\,\text{diffusion}} = 1.900$. The $^{18}\varepsilon_{\text{diffusion}}$ value is derived by raising the measured $^{18}\alpha$ value for kinetic fractionation of O_2 during gas exchange to 3/2 power; the mass dependence is for interdiffusion through 2 water molecules, which is consistent with experimental results in both $^{18}\varepsilon_{\text{diffusion}}$ and θ values [29, 117]. For enzymatic fractionation, we use $\theta_{17/18,\,\text{enzyme}} = 0.5233$, $\theta_{35/34,\,\text{enzyme}} = 1.555$, and $\theta_{36/34,\,\text{enzyme}} = 2.061$, the simplified bond-breaking mass dependence, which has $\theta_{35/34}$ and $\theta_{36/34}$ values between that of heme-O_2 binding and one-electron reduction of O_2^- while

40

keeping a similar $\theta_{17/18}$ value. The results of this model over a range of $^{18}\varepsilon_{enzyme}$ values are shown in Fig. 8.
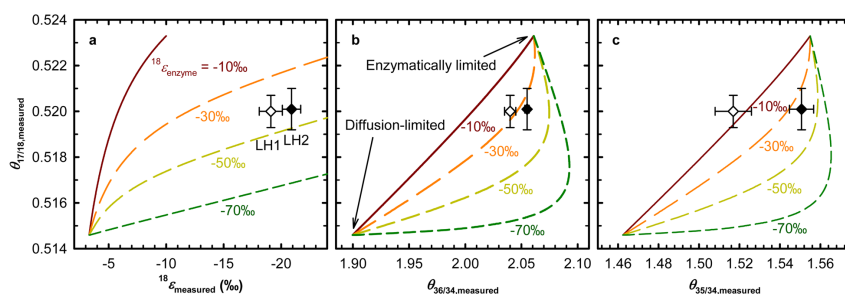

Figure 8. Results of two-step diffusion-enzymatic reduction model for isotopologue fractionation. Cross-plots are shown of the predicted covariations of $\theta_{17/18,measured}$ with (a) $^{18}\varepsilon_{measured}$, (b) $\theta_{36/34,measured}$, and (c) $\theta_{35/34,measured}$, together with experimental results.

We find that our experimental data are generally consistent with natural respiration expressing some diffusion limitation (i.e., implied $r > 0.4$). Nearly all the isotopologue fractionation factors can be explained simultaneously if the combined $^{18}\varepsilon_{enzyme}$ value is between -30‰ and -40‰: Fig. 8 shows all our measurements are within 1σ of this envelope with one exception. The exception is $\theta_{35/34,resp}$ in experiment LH1; in that experiment, that the expected change in Δ_{35} values is near the limits of detection, so the uncertainty in the experimental $\theta_{35/34,resp}$ value may be underestimated. Moreover, a kinetic $^{18}\varepsilon_{enzyme}$ value of this magnitude is plausible as the cumulative fractionation for binding and reduction, or for an outer-sphere quantum-mechanical electron-transfer step to O_2.[114] The specific mechanism that applies to this system, however, awaits further investigation. Interestingly, the covariation of $^{18}\varepsilon_{measured}$ and $\theta_{17/18,resp}$ with changes in temperature reported by Stolper et al. (2018) can be explained qualitatively by this two-step

model if the diffusion limitation becomes less important at higher temperature, where molecular transport is expected to be faster.

In contrast, the lower range of $\theta_{17/18,resp}$ values can only be explained by the model if the reaction occurs closer to the diffusion limit, e.g., $r \sim 0.2$ or less, and the intrinsic enzymatic $^{18}O/^{16}O$ fractionation is much stronger, e.g., $^{18}\varepsilon_{enzyme} \sim$ -70‰. To our knowledge, such large $^{18}O/^{16}O$ fractionation has not been observed before in a non-photochemical system. Well-stirred experiments with isolated enzymes may shed light on which of these cases is more accurate.

An alternative model for isotopic fractionation could invoke a competition between O_2 binding and reduction, wherein proton-transfer limitation expresses lower θ values approaching $\theta_{17/18} = 0.516$, $\theta_{35/34} = 1.5$, and $\theta_{36/34} = 2.0$. In this case, the range of experimental θ values we observe can be fully explained, while the low experimental $\theta_{17/18,resp}$ values previously reported cannot.

While both modeled scenarios have some uncertainty associated with the θ values used for each step, they both favor higher $\theta_{17/18,resp}$ values as being more plausible. The rate-limiting heme-O_2 interaction in other terminal oxidases would have to be fundamentally different from that in Cytochrome c oxidase (i.e., it does not involve O-O bond weakening) for lower $\theta_{17/18,resp}$ values to be defensible based on the molecular mechanism of respiratory O_2 consumption.

New Ar-free oxygen isotopologue observations in the deep ocean may also constrain whether high or low $\theta_{17/18,resp}$ values are expressed in nature. Earlier studies showed highly variable $\Delta'^{17}O$ values in low-O_2 waters—spanning over 200 ppm—that were interpreted as mixtures of high- and low-O_2 components.[18, 55, 118] However, the low-O_2 endmembers had never been observed, rendering this interpretation somewhat speculative. Previous measurements were made on O_2 + Ar mixtures, which may have been susceptible to "pressure baseline" errors and variability therein, so they may need revision.

42

Conclusions and implications for determinations of primary productivity

Our results raise questions about the accuracy of the "canonical" $\theta_{17/18,resp}$ range near 0.515. The Lake Houston incubations, at face value, suggest that the natural $\theta_{17/18,resp}$ value could be 0.004 higher. If true, they imply that existing GOP estimates could be ~40% too high (see Fig. 1). Downward revisions in GOP of this magnitude may resolve lingering disagreements between the triple-oxygen method and $H_2{}^{18}O$ incubations and disagreements between O_2 production-to-C fixation ratios observed *in situ* and in cellular physiology studies.[19, 21, 47, 119] They may also change estimates of ecosystem carbon export efficiencies, which are especially important in oligotrophic regions.[54, 120]

However, there may be fortuitous cancellation of errors in the calculation of GOP because the triple-oxygen composition of seawater typically used in those calculations may also be erroneous.[67] Indeed, revising the photosynthetic O_2 endmember to reflect more recent determinations of the triple-oxygen composition of the Vienna Standard Mean Ocean Water-2 (VSMOW2) standard could mitigate the impact of a +0.004 revision in $\theta_{17/18,resp}$ on GOP estimates almost entirely (Fig. 9).[30, 31]

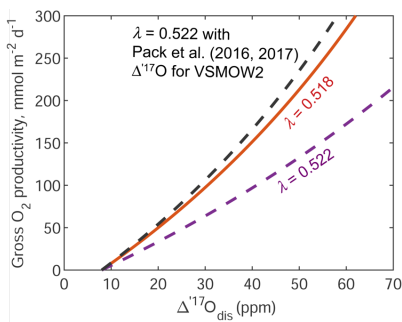**Figure 8. Calculated GOP using the parameters shown in Fig. 1B-C, with effect of VSMOW2 composition overlaid.** Using the $\Delta'^{17}O$ value of VSMOW2 from Pack et al. (2016, 2017) instead of Barkan and Luz (2011) and $\lambda = 0.522$—approximating a closed system in which $^{18}\varepsilon_{resp} \sim -18‰$ and $\theta_{17/18,resp} = 0.520$—results in much smaller changes to GOP ($\lambda = 0.518$) compared to a $\lambda = 0.522$ revision alone.[30, 31, 121]

To what extent marine and global GOP estimates need to be revised, then, will not be known until accurate $\theta_{17/18,resp}$ values, and how they change under different environmental conditions, can be obtained. The reported sensitivity of $\theta_{17/18,resp}$ values to temperature is especially important in this context.[26] Moreover, the use of triple-oxygen isotope variations in various archives to assess past biosphere productivity and to infer the presence of biological activity relies on accurate $\theta_{17/18,resp}$ values and a strong understanding of the factors that modulate its variability.[23-25, 122, 123] Thus, our work highlights the need to re-evaluate both $\theta_{17/18,resp}$ and the triple-isotope composition of the photosynthetic O_2 endmember in new, comprehensive laboratory experiments, and to the extent possible, in theoretical studies.

References

1. Luz, B.; Barkan, E.; Severinghaus, J., The Stable Isotopic Composition of Atmospheric O2. **2014**.

2. Guy, R. D.; Fogel, M. L.; Berry, J. A., Photosynthetic Fractionation of the Stable Isotopes of Oxygen and Carbon. *Plant Physiology* **1993**, *101*, 37-47.

3. Helman, Y.; Barkan, E.; Eisenstadt, D.; Luz, B.; Kaplan, A., Fractionation of the Three Stable Oxygen Isotopes by Oxygen-Producing and Oxygen-Consuming Reactions in Photosynthetic Organisms. *Plant Physiology* **2005**, *138* (4), 2292-2298.

4. Eisenstadt, D.; Barkan, E.; Luz, B.; Kaplan, A., Enrichment of oxygen heavy isotopes during photosynthesis in phytoplankton. *Photosynthesis Research* **2010**, *103*, 97-103.

5. Rakestraw, N. M.; Rudd, D. P.; Dole, M., Isotopic composition of oxygen in air dissolved in Pacific Ocean water as a function of depth. *Journal of the American Chemical Society* **1951**, *73* (6), 2976-2976.

6. Lane, G. A.; Dole, M., Fractionation of oxygen isotopes during respiration. *Science (Washington, D. C., 1883-)* **1956**, *123* (3197), 574-576.

7. Schleser, G. H., Oxygen Isotope Fractionation during Respiration for Different Temperatures of T-Utilis and Escherichia-Coli-K12. *Radiat Environ Bioph* **1979**, *17* (1), 85-93.

8. Guy, R. D.; Berry, J. A.; Fogel, M. L.; Hoering, T. C., Differential fractionation of oxygen isotopes by cyanide-resistant and cyanice-sensitive respiration in plants. *Planta* **1989**, *177*, 483-491.

9.   Epstein, S.; Zeiri, L., Oxygen and Carbon Isotopic Compositions of Gases Respired by Humans. *P Natl Acad Sci USA* **1988,** *85* (6), 1727-1731.

10.   Kiddon, J.; Bender, M. L.; Orchardo, J.; Caron, D. A.; Goldman, J. C.; Dennett, M., Isotopic fractionation of oxygen by respiring marine organisms. *Global Biogeochemical Cycles* **1993,** *7* (3), 679-694.

11.   Angert, A.; Luz, B., Fractionation of oxygen isotopes by root respiration: Implications for the isotopic composition of atmospheric O_2. *Geochim Cosmochim Ac* **2001,** *65* (11), 1695-1701.

12.   Angert, A.; Rachmilevitch, S.; Barkan, E.; Luz, B., Effects of photorespiration, the cytochrome pathway, and the alternative pathway on the triple isotopic composition on atmospheric O_2. *Global Biogeochemical Cycles* **2003,** *17* (1), 1030.

13.   Bender, M.; Sowers, T.; Labeyrie, L., The Dole effect and its variations during the last 130,000 years as measured in the Vostok ice core. *Global Biogeochemical Cycles* **1994,** *8* (3), 363-376.

14.   Heidenreich, J. E.; Thiemens, M. H., A non-mass-dependent isotope effect in the production of ozone from molecular oxygen. *Journal of Chemical Physics* **1983,** *78*, 892-895.

15.   Thiemens, M. H.; Jackson, T.; Zipf, E. C.; Erdman, P. W.; van Egmond, C., Carbon Dioxide and Oxygen Isotope Anomalies in the Mesosphere and Stratosphere. *Science (Washington, D. C., 1883-)* **1995,** *270* (5238), 969-972.

16.   Luz, B.; Barkan, E., Assessment of Oceanic Productivity with the Triple-Isotope Composition of Dissolved Oxygen. *Science (Washington, D. C., 1883-)* **2000,** *288* (5473), 2028-2031.

46

17. Hendricks, M. B.; Bender, M. L.; Barnett, B. A., Net and gross O_2 production in the Southern Ocean from measurements of biological O_2 saturation and its triple isotope composition. *Deep-Sea Research Part I-Oceanographic Research Papers* **2004,** *51* (11), 1541-1561.

18. Hendricks, M. B.; Bender, M. L.; Barnett, B. A.; Strutton, P.; Chavez, F. P., Triple oxygen isotope composition of dissolved O_2 in the equatorial Pacific: A tracer of mixing, production, and respiration. *Journal of Geophysical Research* **2005,** *110* (C12), C12021.

19. Quay, P. D.; Peacock, C.; Bjorkman, K.; Karl, D. M., Measuring primary production rates in the ocean: Enigmatic results between incubation and non-incubation methods at Station ALOHA. *Global Biogeochemical Cycles* **2010,** *24*, GB3014.

20. Stanley, R. H. R.; Kirkpatrick, J. B.; Cassar, N.; Barnett, B.; Bender, M. L., Net community production and gross primary production rates in the western equatorial pacific. *Global Biogeochemical Cycles* **2010,** *24*, GB4001.

21. Juranek, L. W.; Quay, P. D., Using Triple Isotopes of Dissolved Oxygen to Evaluate Global Marine Productivity. *Annual Review of Marine Science* **2013,** *5*, 503-524.

22. Prokopenko, M. G.; Pauluis, O. M.; Granger, J.; Yeung, L. Y., Exact evaluation of gross photosynthetic production from the oxygen triple-isotope composition of O_2: Implications for the net-to-gross primary production ratios. *Geophys Res Lett* **2011,** *38*, L14603.

23. Luz, B.; Barkan, E.; Bender, M. L.; Thiemens, M. H.; Boering, K. A., Triple-isotope composition of atmospheric oxygen as a tracer of biosphere productivity. *Nature (London)* **1999,** *400* (6744), 547-550.

24. Blunier, T.; Barnett, B.; Bender, M. L.; Hendricks, M. B., Biological oxygen productivity during the last 60,000 years from triple oxygen isotope measurements. *Global Biogeochemical Cycles* **2002,** *16* (3), 1029.

25. Blunier, T.; Bender, M. L.; Barnett, B.; von Fischer, J. C., Planetary fertility during the past 400 ka based on the triple isotope composition of O_2 in trapped gases from the Vostok ice core. *Climate of the Past* **2012,** *8*, 1509-1526.

26. Stolper, D. A.; Fischer, W. W.; Bender, M. L., Effects of temperature and carbon source on the isotopic fractionations associated with O2 respiration for 17O/16O and 18O/16O ratios in E. coli. *Geochim Cosmochim Ac* **2018,** *240*, 152-172.

27. Yeung, L. Y.; Hayles, J. A.; Hu, H.; Ash, J. L.; Sun, T., Scale distortion from pressure baselines as a source of inaccuracy in triple-isotope measurements. *Rapid Communications in Mass Spectrometry* **2018,** *32* (20), 1811-1821.

28. Yeung, L. Y.; Young, E. D.; Schauble, E. A., Measurements of $^{18}O^{18}O$ and $^{17}O^{18}O$ in the atmosphere and the influence of isotope-exchange reactions. *Journal of Geophysical Research* **2012,** *117*, D18306.

29. Li, B.; Hu, H.; Ash, J. L.; Yeung, L. Y., Kinetic and equilibrium fractionation of O_2 isotopologues during air-water gas transfer and implications for tracing oxygen cycling in the ocean. *Marine Chemistry* **2019,** *In revision*.

30. Pack, A.; Höweling, A.; Hezel, D. C.; Stefanak, M. T.; Beck, A.-K.; Peters, S. T.; Sengupta, S.; Herwartz, D.; Folco, L., Tracing the oxygen isotope composition of the upper Earth's atmosphere using cosmic spherules. *Nature communications* **2017,** *8*, 15702.

31. Pack, A.; Tanaka, R.; Hering, M.; Sengupta, S.; Peters, S.; Nakamura, E., The oxygen isotope composition of San Carlos olivine on the VSMOW2-SLAP2 scale. *Rapid Communications in Mass Spectrometry* **2016,** *30* (13), 1495-1504.

32. Dauphas, N.; Schauble, E. A., Mass fractionation laws, mass-independent effects, and isotopic anomalies. *Annual Review of Earth and Planetary Sciences* **2016,** *44*, 709-783.

33. Young, E. D.; Galy, A.; Nagahara, H., Kinetic and equilibrium mass-dependent isotope fractionation laws in nature and ther geochemical and cosmochemical significance. *Geochim Cosmochim Ac* **2002,** *66* (6), 1095-1104.

34. Clayton, R. N.; Grossman, L.; Mayeda, T. K., A Component of Primitive Nuclear Composition in Carbonaceous Meteorites. *Science (Washington, D. C., 1883-)* **1973,** *182* (4111), 485-488.

35. Barkan, E.; Luz, B., High precision measurements of $^{17}O/^{16}O$ and $^{18}O/^{16}O$ ratios in H_2O. *Rapid Communications in Mass Spectrometry* **2005,** *19*, 3737-3742.

36. Pack, A.; Herwartz, D., The triple oxygen isotope composition of the Earth mantle and understanding $\Delta O17$ variations in terrestrial rocks and minerals. *Earth and Planetary Science Letters* **2014,** *390*, 138-145.

37. Bao, H.; Fairchild, I. J.; Wynn, P. M.; Spötl, C., Stretching the envelope of past surface environments: Neoproterozoic glacial lakes from Svalbard. *Science* **2009,** *323* (5910), 119-122.

38. Young, E. D.; Kohl, I. E.; Warren, P. H.; Rubie, D. C.; Jacobson, S. A.; Morbidelli, A., Oxygen isotopic evidence for vigorous mixing during the Moon-forming giant impact. *Science* **2016,** *351* (6272), 493-496.

39.   Luz, B.; Barkan, E., Net and gross oxygen production from O_2/Ar, $^{17}O/^{16}O$, and $^{18}O/^{16}O$ ratios. *Aquatic Microbial Ecology* **2009,** *56* (2-3), 133-145.

40.   Urey, H. C.; Grieff, L. J., Isotopic exchange equilibria. *Journal of the American Chemical Society* **1935,** *57*, 321-327.

41.   Bigeleisen, J.; Mayer, M. G., Calculation of equilibrium constants for isotopic exchange reactions. *Journal of Chemical Physics* **1947,** *15* (5), 261-267.

42.   Cao, X.; Liu, Y., Equilibrium mass-dependent fractionation relationships for triple oxygen isotopes. *Geochim Cosmochim Ac* **2011,** *75* (23), 7435-7445.

43.   Bao, H.; Cao, X.; Hayles, J. A., Triple oxygen isotopes: fundamental relationships and applications. *Annual Review of Earth and Planetary Sciences* **2016,** *44*, 463-492.

44.   Luz, B.; Barkan, E., The isotopic ratios $^{17}O/^{16}O$ and $^{18}O/^{16}O$ in molecular oxygen and their significance in biogeochemistry. *Geochim Cosmochim Ac* **2005,** *69* (5), 1099-1110.

45.   Yung, Y. L.; DeMore, W. B.; Pinto, J. P., Isotopic Exchange Between Carbon Dioxide and Ozone via $O(^1D)$ in the Stratosphere. *Geophys Res Lett* **1991,** *18* (1), 13-16.

46.   Boering, K. A.; Jackson, T.; Hoag, K. J.; Cole, A. S.; Perri, M. J.; Thiemens, M.; Atlas, E., Observations of the anomalous oxygen isotopic composition of carbon dioxide in the lower stratosphere and the flux of the anomaly to the troposphere. *Geophys Res Lett* **2004,** *31* (3), L03109.

47.   Juranek, L. W.; Quay, P. D., In vitro and in situ gross primary and net community production in the North Pacific Subtropical Gyre using labeled and natural abundance isotopes of dissolved O_2. *Global Biogeochemical Cycles* **2005,** *19* (3), 15.

48.   Juranek, L. W.; Quay, P. D., Basin-wide photosynthetic production rates in the subtropical and tropical Pacific Ocean determined from dissolved oxygen isotope ratio measurements. *Global Biogeochemical Cycles* **2010,** *24*, GB2006.

49.   Reuer, M. K.; Barnett, B. A.; Bender, M. L.; Falkowski, P. G.; Hendricks, M. B., New estimates of Southern Ocean biological production rates from O_2/Ar ratios and the triple isotope composition of O_2. *Deep-Sea Research Part I-Oceanographic Research Papers* **2007,** *54* (6), 951-974.

50.   Bender, M.; Grande, K.; Johnson, K.; Marra, J.; Williams, P. J. L.; Sieburth, J.; Pilson, M.; Langdon, C.; Hitchcock, G.; Orchardo, J.; Hunt, C.; Donaghay, P.; Heinemann, K., A comparison of 4 methods for determining planktonic community production. *Limnol Oceanogr* **1987,** *32* (5), 1085-1098.

51.   Sarma, V.; Abe, O.; Hinuma, A.; Saino, T., Short-term variation of triple oxygen isotopes and gross oxygen production in the Sagami Bay, central Japan. *Limnol Oceanogr* **2006,** *51* (3), 1432-1442.

52.   Palevsky, H. I.; Quay, P. D.; Nicholson, D. P., Discrepant estimates of primary and export production from satellite algorithms, a biogeochemical model, and geochemical tracer measurements in the North Pacific Ocean. *Geophys Res Lett* **2016,** *43* (16), 8645-8653.

53. Luz, B.; Barkan, E.; Sagi, Y.; Yacobi, Y. Z., Evaluation of community respiratory mechanisms with oxygen isotopes: A case study in Lake Kinneret. *Limnol Oceanogr* **2002,** *47* (1), 33-42.

54. Nicholson, D. P.; Stanley, R. H. R.; Barkan, E.; Karl, D. M.; Luz, B.; Quay, P. D.; Doney, S. C., Evaluating triple oxygen isotope estimates of gross primary production at the Hawaii Ocean Time-series and Bermuda Atlantic Time-series Study sites. *Journal of Geophysical Research* **2012,** *117*, C05012.

55. Nicholson, D.; Stanley, R. H. R.; Doney, S. C., The triple oxygen isotope tracer of primary productivity in a dynamic ocean model. *Global Biogeochemical Cycles* **2014,** *28*, doi: 10.1002/2013GB004704.

56. Ho, D. T.; Wanninkhof, R.; Schlosser, P.; Ullman, D. S.; Hebert, D.; Sullivan, K. F., Toward a universal relationship between wind speed and gas exchange: Gas transfer velocities measured with ^{3}He/SF$_6$ during the Southern Ocean Gas Exchange Experiment. *Journal of Geophysical Research* **2011,** *116*, C00F04.

57. Yeung, L. Y.; Ash, J. L.; Young, E. D., Biological signatures in clumped isotopes of O$_2$. *Science* **2015,** *348* (6233), 431-434.

58. Kaiser, J., Technical note: Consistent calculation of aquatic gross production from oxygen triple isotope measurements. *Biogeosciences* **2011,** *8*, 1793-1811.

59. Nicholson, D. P., Comment on: "Technical note: Consistent calculation of aquatic gross production from oxygen triple isotope measurements" by Kaiser (2011). *Biogeosciences* **2011,** *8*, 2993-2997.

60.   Manning, C. C.; Howard, E. M.; Nicholson, D. P.; Ji, B. Y.; Sandwith, Z. O.; Stanley, R. H., Revising estimates of aquatic gross oxygen production by the triple oxygen isotope method to incorporate the local isotopic composition of water. *Geophys Res Lett* **2017,** *44* (20), 10,511-10,519.

61.   Luz, B.; Barkan, E., Proper estimation of marine gross O_2 production with $^{17}O/^{16}O$ and $^{18}O/^{16}O$ ratios of dissolved O_2. *Geophys Res Lett* **2011,** *38*, L19606.

62.   Eiler, J. M., "Clumped-isotope" geochemistry -- The study of naturally-occurring, multiply-substituted isotopologues. *Earth and Planetary Science Letters* **2007,** *262*, 309-327.

63.   Yeung, L. Y.; Murray, L. T.; Martinerie, P.; Witrant, E.; Hu, H.; Banerjee, A.; Orsi, A.; Chappellaz, J., Isotopic constraint on the twentieth-century increase in tropospheric ozone. *Nature* **2019,** *570* (7760), 224.

64.   Kirkwood, D. S., Stability of solutions of nutrient salts during storage. *Marine Chemistry* **1992,** *38*, 151-164.

65.   Yeung, L. Y.; Murray, L. T.; Ash, J. L.; Young, E. D.; Boering, K. A.; Atlas, E. L.; Schauffler, S. M.; Lueb, R. A.; Langenfelds, R. L.; Krummel, P., Isotopic ordering in atmospheric O_2 as a tracer of ozone photochemistry and the tropical atmosphere. *Journal of Geophysical Research: Atmospheres* **2016,** *121* (20).

66.   Yeung, L. Y.; Ash, J. L.; Young, E. D., Rapid photochemical equilibration of isotope bond ordering in O_2. *Journal of Geophysical Research* **2014,** *119*, 10,552-10566.

67.   Young, E. D.; Yeung, L. Y.; Kohl, I. E., On the $\Delta^{17}O$ Budget of Atmospheric O_2. *Geochim Cosmochim Ac* **2014,** *135*, 102-125.

68. Urey, H. C., The thermodynamic properties of isotopic substances. *Journal of the Chemical Society* **1947,** *47* (5), 562-581.

69. Solomon, E. I.; Heppner, D. E.; Johnston, E. M.; Ginsbach, J. W.; Cirera, J.; Qayyum, M.; Kieber-Emmons, M. T.; Kjaergaard, C. H.; Hadt, R. G.; Tian, L., Copper Active Sites in Biology. *Chem Rev* **2014,** *114* (7), 3659-3853.

70. Blomberg, M. R. A.; Borowski, T.; Himo, F.; Liao, R.-Z.; Siegbahn, P. E. M., Quantum Chemical Studies of Mechanisms for Metalloenzymes. *Chem Rev* **2014,** *114* (7), 3601-3658.

71. Kepp, K. P.; Dasmeh, P., Effect of Distal Interactions on O_2 Binding to Heme. *The Journal of Physical Chemistry B* **2013,** *117* (14), 3755-3770.

72. Wikström, M.; Krab, K.; Sharma, V., Oxygen Activation and Energy Conservation by Cytochrome c Oxidase. *Chem Rev* **2018,** *118* (5), 2469-2490.

73. Smirnov, V. V.; Lanci, M. P.; Roth, J. P., Computational Modeling of Oxygen Isotope Effects on Metal-Mediated O2 Activation at Varying Temperatures. *The Journal of Physical Chemistry A* **2009,** *113* (10), 1934-1945.

74. Schaefer, A. W.; Roveda, A. C.; Jose, A.; Solomon, E. I., Geometric and Electronic Structure Contributions to O–O Cleavage and the Resultant Intermediate Generated in Heme-Copper Oxidases. *Journal of the American Chemical Society* **2019,** *141* (25), 10068-10081.

75. Schuth, N.; Mebs, S.; Huwald, D.; Wrzolek, P.; Schwalbe, M.; Hemschemeier, A.; Haumann, M., Effective intermediate-spin iron in O_2-transporting heme proteins. *P Natl Acad Sci USA* **2017,** *114* (32), 8556-8561.

76.   Blomberg, M. R. A.; Siegbahn, P. E. M.; Wikström, M., Metal-Bridging Mechanism for O–O Bond Cleavage in Cytochrome c Oxidase. *Inorganic Chemistry* **2003,** *42* (17), 5231-5243.

77.   Becke, A. D., Density-functional thermochemistry. III. The role of exact exchange. *The Journal of Chemical Physics* **1993,** *98* (7), 5648-5652.

78.   Lee, C.; Yang, W.; Parr, R. G., Development of the Colle-Salvetti correlation-energy formula into a functional of the electron density. *Physical Review B* **1988,** *37* (2), 785-789.

79.   Grimme, S.; Ehrlich, S.; Goerigk, L., Effect of the damping function in dispersion corrected density functional theory. *Journal of Computational Chemistry* **2011,** *32* (7), 1456-1465.

80.   Tao, J.; Perdew, J. P.; Staroverov, V. N.; Scuseria, G. E., Climbing the Density Functional Ladder: Nonempirical Meta--Generalized Gradient Approximation Designed for Molecules and Solids. *Physical Review Letters* **2003,** *91* (14), 146401.

81.   Staroverov, V. N.; Scuseria, G. E.; Tao, J.; Perdew, J. P., Comparative assessment of a new nonempirical density functional: Molecules and hydrogen-bonded complexes. *The Journal of Chemical Physics* **2003,** *119* (23), 12129-12137.

82.   Peverati, R.; Zhao, Y.; Truhlar, D. G., Generalized Gradient Approximation That Recovers the Second-Order Density-Gradient Expansion with Optimized Across-the-Board Performance. *The Journal of Physical Chemistry Letters* **2011,** *2* (16), 1991-1997.

83.   Weigend, F.; Ahlrichs, R., Balanced basis sets of split valence, triple zeta valence and quadruple zeta valence quality for H to Rn: Design and assessment of accuracy. *Physical Chemistry Chemical Physics* **2005,** *7* (18), 3297-3305.

84.   Jensen, K. P.; Roos, B. O.; Ryde, U., Performance of density functionals for first row transition metal systems. *The Journal of Chemical Physics* **2007,** *126* (1), 014103.

85.   Siegbahn, P. E. M.; Blomberg, M. R. A.; Chen, S.-L., Significant van der Waals Effects in Transition Metal Complexes. *Journal of Chemical Theory and Computation* **2010,** *6* (7), 2040-2044.

86.   Jensen, K. P., Bioinorganic Chemistry Modeled with the TPSSh Density Functional. *Inorganic Chemistry* **2008,** *47* (22), 10357-10365.

87.   Perdew, J. P.; Burke, K.; Ernzerhof, M., Generalized Gradient Approximation Made Simple. *Physical Review Letters* **1996,** *77* (18), 3865-3868.

88.   Zhao, Y.; Truhlar, D. G., Construction of a generalized gradient approximation by restoring the density-gradient expansion and enforcing a tight Lieb–Oxford bound. *The Journal of Chemical Physics* **2008,** *128* (18), 184109.

89.   Kesharwani, M. K.; Brauer, B.; Martin, J. M. L., Frequency and Zero-Point Vibrational Energy Scale Factors for Double-Hybrid Density Functionals (and Other Selected Methods): Can Anharmonic Force Fields Be Avoided? *The Journal of Physical Chemistry A* **2015,** *119* (9), 1701-1714.

90.   Piasecki, A.; Sessions, A.; Peterson, B.; Eiler, J., Prediction of equilibrium distributions of isotopologues for methane, ethane and propane using density functional theory. *Geochim Cosmochim Ac* **2016,** *190*, 1-12.

91. Liu, Q.; Tossell, J. A.; Liu, Y., On the proper use of the Bigeleisen–Mayer equation and corrections to it in the calculation of isotopic fractionation equilibrium constants. *Geochim Cosmochim Ac* **2010,** *74* (24), 6965-6983.

92. Cao, X.; Liu, Y., Theoretical estimation of the equilibrium distribution of clumped isotopes in nature. *Geochim Cosmochim Ac* **2011,** *77*, 292-303.

93. Chance, B.; Saronio, C.; Leigh, J. S., Functional intermediates in the reaction of membrane-bound cytochrome oxidase with oxygen. *Journal of Biological Chemistry* **1975,** *250* (24), 9226-37.

94. Frisch, M. J.; Trucks, G. W.; Schlegel, H. B.; Scuseria, G. E.; Robb, M. A.; Cheeseman, J. R.; Scalmani, G.; Barone, V.; Petersson, G. A.; Nakatsuji, H.; Li, X.; Caricato, M.; Marenich, A. V.; Bloino, J.; Janesko, B. G.; Gomperts, R.; Mennucci, B.; Hratchian, H. P.; Ortiz, J. V.; Izmaylov, A. F.; Sonnenberg, J. L.; Williams; Ding, F.; Lipparini, F.; Egidi, F.; Goings, J.; Peng, B.; Petrone, A.; Henderson, T.; Ranasinghe, D.; Zakrzewski, V. G.; Gao, J.; Rega, N.; Zheng, G.; Liang, W.; Hada, M.; Ehara, M.; Toyota, K.; Fukuda, R.; Hasegawa, J.; Ishida, M.; Nakajima, T.; Honda, Y.; Kitao, O.; Nakai, H.; Vreven, T.; Throssell, K.; Montgomery Jr., J. A.; Peralta, J. E.; Ogliaro, F.; Bearpark, M. J.; Heyd, J. J.; Brothers, E. N.; Kudin, K. N.; Staroverov, V. N.; Keith, T. A.; Kobayashi, R.; Normand, J.; Raghavachari, K.; Rendell, A. P.; Burant, J. C.; Iyengar, S. S.; Tomasi, J.; Cossi, M.; Millam, J. M.; Klene, M.; Adamo, C.; Cammi, R.; Ochterski, J. W.; Martin, R. L.; Morokuma, K.; Farkas, O.; Foresman, J. B.; Fox, D. J. *Gaussian 16 Rev. B.01*, Wallingford, CT, 2016.

95.   Blomberg, M. R. A.; Siegbahn, P. E. M.; Babcock, G. T., Modeling Electron Transfer in Biochemistry: A Quantum Chemical Study of Charge Separation in Rhodobacter sphaeroides and Photosystem II. *Journal of the American Chemical Society* **1998,** *120* (34), 8812-8824.

96.   Rustad, J. R.; Casey, W. H.; Yin, Q.-Z.; Bylaska, E. J.; Felmy, A. R.; Bogatko, S. A.; Jackson, V. E.; Dixon, D. A., Isotopic fractionation of $Mg^{2+(aq)}$, $Ca^{2+(aq)}$, and $Fe^{2+(aq)}$ with carbonate minerals. *Geochim Cosmochim Ac* **2010,** *74* (22), 6301-6323.

97.   Rustad, J. R.; Nelmes, S. L.; Jackson, V. E.; Dixon, D. A., Quantum-Chemical Calculations of Carbon-Isotope Fractionation in CO2(g), Aqueous Carbonate Species, and Carbonate Minerals. *The Journal of Physical Chemistry A* **2008,** *112* (3), 542-555.

98.   Garcia, H. E.; Gordon, L. I., Oxygen solubility in seawater: Better fitting equations. *Limnol Oceanogr* **1992,** *37* (6), 1307-1312.

99.   Hamme, R. C.; Emerson, S. R., The solubility of neon, nitrogen and argon in distilled water and seawater. *Deep Sea Research Part I: Oceanographic Research Papers* **2004,** *51* (11), 1517-1528.

100. Kitagawa, Y.; Saito, T.; Nakanishi, Y.; Ito, M.; Shoji, M.; Koizumi, K.; Yamanaka, S.; Kawakami, T.; Okumura, M.; Yamaguchi, K., Geometry Optimization without Spin Contamination Error - Approximately Spin Projected Optimization Method -. *AIP Conference Proceedings* **2007,** *963* (2), 334-337.

101. Wilson, S. A.; Green, E.; Mathews, I. I.; Benfatto, M.; Hodgson, K. O.; Hedman, B.; Sarangi, R., X-ray absorption spectroscopic investigation of the electronic structure differences

in solution and crystalline oxyhemoglobin. *Proceedings of the National Academy of Sciences* **2013,** *110* (41), 16333-16338.

102. Huber, K. P.; Herzberg, G., *Constants of diatomic molecules*. Van Nostrand Reinhold Company: New York, NY, 1979; p 736.

103. Potter, W. T.; Tucker, M. P.; Houtchens, R. A.; Caughey, W. S., Oxygen infrared spectra of oxyhemoglobins and oxymyoglobins. Evidence of two major liganded oxygen structures. *Biochemistry* **1987,** *26* (15), 4699-4707.

104. Hirota, S.; Ogura, T.; Appelman, E. H.; Shinzawa-Itoh, K.; Yoshikawa, S.; Kitagawa, T., Observation of a New Oxygen-Isotope-Sensitive Raman Band for Oxyhemoproteins and Its Implications in Heme Pocket Structures. *Journal of the American Chemical Society* **1994,** *116* (23), 10564-10570.

105. Ogura, T.; Takahashi, S.; Hirota, S.; Shinzawa-Itoh, K.; Yoshikawa, S.; Appelman, E. H.; Kitagawa, T., Time-resolved resonance Raman elucidation of the pathway for dioxygen reduction by cytochrome c oxidase. *Journal of the American Chemical Society* **1993,** *115* (19), 8527-8536.

106. Berger, A. J.; Wang, Y.; Sammeth, D. M.; Itzkan, I.; Kneipp, K.; Feld, M. S., Aqueous Dissolved Gas Measurements Using Near-Infrared Raman Spectroscopy. *Appl*. *Spectrosc*. **1995,** *49* (8), 1164-1169.

107. Tian, G.; Berry, J. A.; Klinman, J. P., Oxygen-18 kinetic isotope effects in the dopamine .beta.-monooxygenase reaction: Evidence for a new chemical mechanism in non-heme, metallomonooxygenase. *Biochemistry* **1994,** *33* (1), 226-234.

59

108. Knox, M.; Quay, P. D.; Wilbur, D., Kinetic isotope fractionation during air-water gas transfer of O_2, N_2, CH_4, and H_2. *Journal of Geophysical Research* **1992,** *97* (C12), 20,335-20,343.

109. Doornkamp, C.; Clement, M.; Ponec, V., The Isotopic Exchange Reaction of Oxygen on Metal Oxides. *Journal of Catalysis* **1999,** *182* (2), 390-399.

110. Möller, M. N.; Li, Q.; Chinnaraj, M.; Cheung, H. C.; Lancaster, J. R.; Denicola, A., Solubility and diffusion of oxygen in phospholipid membranes. *Biochimica et Biophysica Acta (BBA) - Biomembranes* **2016,** *1858* (11), 2923-2930.

111. Poiana, F.; von Ballmoos, C.; Gonska, N.; Blomberg, M. R. A.; Ädelroth, P.; Brzezinski, P., Splitting of the O–O bond at the heme-copper catalytic site of respiratory oxidases. *Science Advances* **2017,** *3* (6), e1700279.

112. Verkhovsky, M. I.; Morgan, J. E.; Wikstroem, M., Oxygen Binding and Activation: Early Steps in the Reaction of Oxygen with Cytochrome c Oxidase. *Biochemistry* **1994,** *33* (10), 3079-3086.

113. Verkhovsky, M. I.; Morgan, J. E.; Puustinen, A.; Wikström, M., Kinetic trapping of oxygen in cell respiration. *Nature* **1996,** *380* (6571), 268-270.

114. Roth, J. P.; Wincek, R.; Nodet, G.; Edmondson, D. E.; McIntire, W. S.; Klinman, J. P., Oxygen Isotope Effects on Electron Transfer to O2 Probed Using Chemically Modified Flavins Bound to Glucose Oxidase. *Journal of the American Chemical Society* **2004,** *126* (46), 15120-15131.

115. Shiba, T.; Inaoka, D. K.; Takahashi, G.; Tsuge, C.; Kido, Y.; Young, L.; Ueda, S.; Balogun, E. O.; Nara, T.; Honma, T.; Tanaka, A.; Inoue, M.; Saimoto, H.; Harada, S.; Moore, A. L.; Kita, K., Insights into the ubiquinol/dioxygen binding and proton relay pathways of the alternative oxidase. *Biochimica et Biophysica Acta (BBA) - Bioenergetics* **2019,** *1860* (5), 375-382.

116. Janik, I.; Tripathi, G. N. R., The nature of the superoxide radical anion in water. *The Journal of Chemical Physics* **2013,** *139* (1), 014302.

117. Jähne, B.; Haussbecker, H., Air-water gas exchange. *Annual Review of Fluid Mechanics* **1998,** *30*, 443-468.

118. Haskell, W. Z.; Prokopenko, M. G.; Hammond, D. E.; Stanley, R. H. R.; Sandwith, Z. O., Annual Cyclicity in Export Efficiency in the Inner Southern California Bight. *Global Biogeochemical Cycles* **2017**, n/a-n/a.

119. Halsey, K. H.; Jones, B. M., Phytoplankton Strategies for Photosynthetic Energy Allocation. *Annual Review of Marine Science* **2015,** *7* (1), 265-297.

120. Bender, M. L.; Dickson, M.-L.; Orchardo, J., Net and gross production in the Ross Sea as deterined by incubation experiments and dissolved O_2 studies. *Deep-Sea Research Part Ii-Topical Studies in Oceanography* **2000,** *47*, 3141-3158.

121. Barkan, E.; Luz, B., The relationships among the three stable isotopes of oxygen in air, seawater and marine photosynthesis. *Rapid Communications in Mass Spectrometry* **2011,** *25* (16), 2367-2369.

122. Crockford, P. W.; Hayles, J. A.; Bao, H.; Planavsky, N. J.; Bekker, A.; Fralick, P. W.; Halverson, G. P.; Bui, T. H.; Peng, Y.; Wing, B. A., Triple oxygen isotope evidence for limited mid-Proterozoic primary productivity. *Nature* **2018,** *559* (7715), 613-616.

123. Christensen, J.;   Kohl, I.; Coleman, M. L. In *P42C-10: Triple oxygen isotope data characterize oxidation processes that produce sulfate on Earth (and Mars?)*, American Geophysical Union Fall Meeting, San Francisco, CA, San Francisco, CA, 2011.